A Riemannian Distance Approach to Probing Signal Design for MIMO Radar

A RIEMANNIAN DISTANCE APPROACH TO PROBING SIGNAL DESIGN FOR MIMO RADAR

BY

YUHENG ZHOU, B.Sc.

A THESIS

SUBMITTED TO THE DEPARTMENT OF ELECTRICAL & COMPUTER ENGINEERING

AND THE SCHOOL OF GRADUATE STUDIES

OF MCMASTER UNIVERSITY

IN PARTIAL FULFILMENT OF THE REQUIREMENTS

FOR THE DEGREE OF

MASTER OF APPLIED SCIENCE

Master of Applied Science (2016) McMaster University

(Electrical & Computer Engineering) Hamilton, Ontario, Canada

TITLE:	A Riemannian Distance Approach to Probing Signal Design for MIMO Radar
AUTHOR:	Yuheng Zhou B.Sc., (Electrical Engineering) McMaster University, Hamilton, Canada
SUPERVISOR:	Dr. K. M. Wong, Dr. T. N. Davidson
NUMBER OF PAGES:	xv, 81

To my family and my friends

Abstract

We consider the problem of designing probing signals for a Multi-Input Multi-Output (MIMO) radar. The goal is to design a signal vector having a desired covariance while ensuring the sidelobes of the ambiguity functions are small. We will also consider cases in which a bandwidth constraint is placed on the signal. Since covariance matrices are structurally constrained, they form a manifold in the signal space. Hence, we argue that the difference between these matrices should not be measured in terms of the conventional Euclidean distance (ED), rather, the distance should be measured along the surface of the manifold, i.e., in terms of a Riemannian distance (RD). An optimization problem for the design of the probing signal is formulated for each distance metric, with the waveform being represented as a linear combination of a set of orthonormal signals. In both cases, the optimization problem is quartic in the coefficients. An efficient algorithm based on iterative convex quadratic optimization is developed and is effective in producing good solutions. In addition, we show that by optimizing over the manifold, the number of iterations can be significantly reduced in comparison to optimizing in the Euclidean space. Several orthonormal signal sets are used in our design examples, including the Walsh functions, the cosine functions and a set of functions designed for optimal time-frequency concentration. When the time-frequency constraints are tight, the selection of the orthonormal set plays a significant

role in the design, with the functions with optimal time-frequency concentration.

Acknowledgements

I would like to express my sincere thanks of gratitude to people who have helped me and supported me to complete my thesis for the program of Master of Applied Science at McMaster University.

First and foremost, I would like to express my gratitude to my supervisors, Dr. Kon Max Wong and Dr. Tim Davidson. I would like to thank Dr. Kon Max Wong for his patience, motivation and immense knowledge. He has offered me inspiring suggestions and continuous encouragement since the first day of research and put great effort to train me in the scientific field. I would also like to thank the other supervisor Dr. Tim Davidson for his valuable advices and guidance. Without their tremendous help and coaching, my academic accomplishment would not have been possible.

Secondly, I would like to thank my group member Jia Xu for her cooperation in completing the conference paper and other group members for their precious friendship.

Thirdly, I would like to thank McMaster University. I have learned knowledge, met great people and enjoyed my student life here.

Last but not the least, I want to say thank you to my family for their endless love and continuous supports.

Notation and Abbreviations

Notations

$\mathbf{A}$	Matrices
$\mathbf{a}$	Vectors
$(\cdot)^T$	Matrix transpose
$(\cdot)^*$	Matrix complex conjugate
$(\cdot)^H$	Matrix hermitian
$\mathbf{I}_M$	$M \times M$ identity matrix
$\mathbb{R}$	Field of real numbers
$\mathbb{C}$	Field of complex numbers
$d(\cdot \ \cdot)$	Distance between two points
$d_E(\cdot \ \cdot)$	Euclidean distance between two points
$d_R(\cdot \ \cdot)$	Riemannian distance between two points
$\hat{d}(\cdot \ \cdot)$	Distance between a point and an approximation of another one
$\mathrm{tr}(\cdot)$	Trace of matrices
$[\mathbf{A}]_{ij}$	The entry in the ith row and jth column
$\mathcal{M}$	Manifold
$\mathcal{H}$	Euclidean space of complex matrixes

$\mathcal{U}_{\mathcal{H}}$	Euclidean subspace space
$\mathcal{T}_{\mathcal{M}}$	Tangent space in $\mathcal{M}$
δ_{kl}	Kronecker delta: 1, if $k = l$; otherwise 0
$\|\cdot\|_F$	Frobenious norm of a vector or a matrix
$\|\cdot\|$	Norm of a constant
$\boldsymbol{A}^{(n)}$	The matrix of nth interation
$\check{\boldsymbol{A}}$	An intermediate solution for a convex quadratic problem
$\mathcal{F}[\cdot]$	Fourier transform
$D[\cdot]$	Time limiting operater
$\mathscr{L}^2$	The space of all square integrable functions in $(-\infty, \infty)$
$\boldsymbol{H}(1:M,:)$	First M rows of matrix $\boldsymbol{H}$

Abbreviations

CA	Cyclic Algorithms
ED	Euclidean Distance
DPSS	Discrete prolate spheroidal sequence
MI	Mutual information
MIMO	Multiple-Input Multiple-Output
PAR	Low peak-to-average-power ratio
PSD	Positive Semidefinite
PSW	Prolate Spheroidal Wave
RD	Riemannian Distance
SIMO	Single-Input Multiple-Ouput

SISO	Single-In Single-Out
SNR	Signal to Noise Ratio

Contents

List of Figures

Chapter 1

Introduction and Problem Statement

1.1 A Radar System

The word *radar* is derived from the phrase "radio detection and ranging". A radar system sends out radio (electromagnetic) waves from a transmitter and collects reflected measureable radio energy from the objects to be seen by a receiver which is typically located at the same site as the transmitter for convenience [3]. The targets of interested to the radar may be aircraft, ships, vehicles, people, meteorological phenomena, or geographical features, and the parameters include locations, directions and velocities of movements [5]. A simple model of an active radar system is shown in Figure 1.1. The transmitted electromagnetic wave is sent from the transmitter and propages through a particular medium. If a target is present, the transmitted signal is reflected and the properties of the reflection are due to the characteristics of the target, such as shape and motion. Ideally, the only distortion is an additive Gaussian

receiver noise. However, in more general cases there is other interferrence, such as reflections from other targets, or layers in the atmosphere [2].

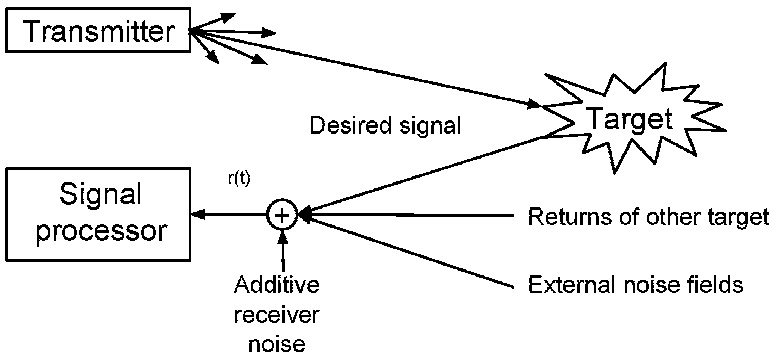

Figure 1.1: Model of an active radar system space[2]

In pulse radar, the transmitter sends out a pulse, and then the receiver is activated. The echoes are reflected back from the targets and are received at different times due to the different propagation delays. When sufficient time has elapsed so that the echoes from the most distant target has returned, the system sends out another pulse and the cycle repeats [3]. Figure 1.2 illustrates the principle of a simple pulse radar.

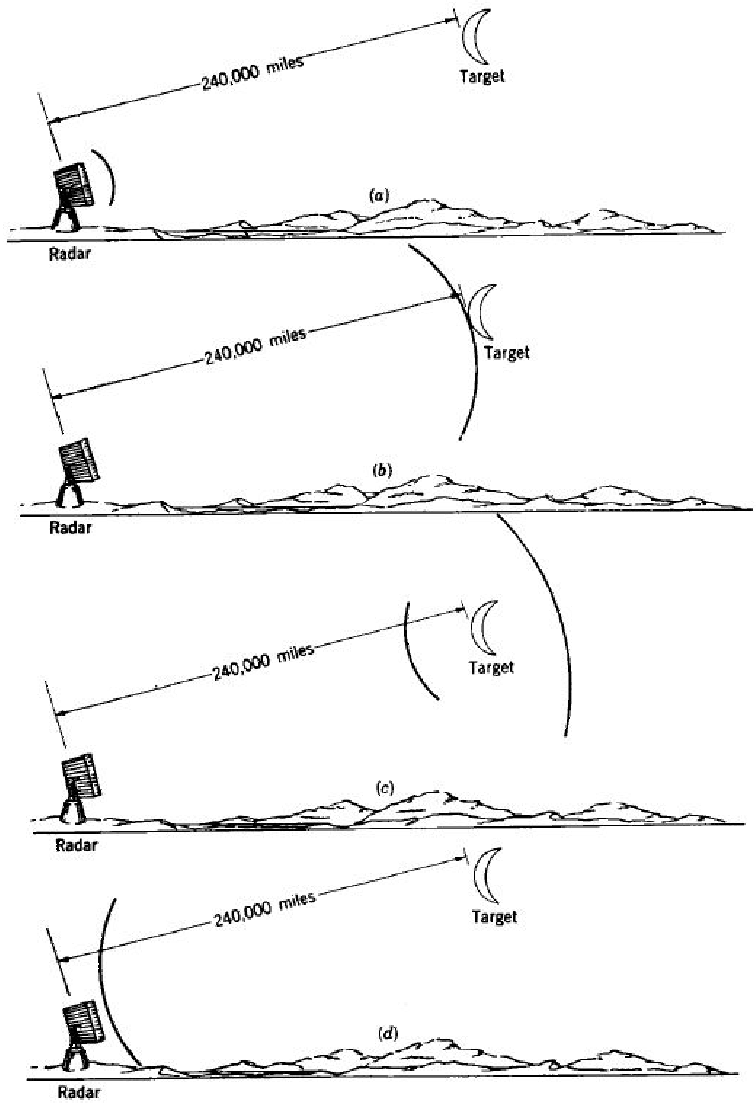

Figure 1.2: The principle of pulse radar. (a) Pulse has just been emitted from radar. (b) Pulse reaches target. (c) Scattered energy returns from target; transmitted pulse carried on. (d) Echo pulse reaches radar [3]

1.2 Importance of MIMO Radar System

Radar systems have been developing rapidly in the past decades and have gone through generations from Single-Input Single-Output (SISO) systems to Multiple Input Multiple Output (MIMO) systems. The example model in previous section is a SISO system which consists of only one tranmitter antenna at the source and one receiver antenna at the destination. Although the system has the advantage of simplicity, the lack of diversity in the single transmitted signal leaves the system exposed to scattering and multipath propagation, resulting fading, losses and attenuation. By increasing the number of receiving antennas, Single-Input Multiple-Output (SIMO) systems can combat the effects of ionospheric fading and interference. Phased array radar is an example of a SIMO system; it transmits scaled versions of a single waveform from each antenna, and have the outputs form each antenna are perfectly correlated [5]. Different from SIMO systems, MIMO radar systems transmit different signals from multiple spatially diverse antennas. The system transmits signals from multiple antennas at source and the returned signals can be extracted by a set of matched filter receivers. The transmitted signals from the anntennas at source are orthogonal (or incoherent) so that it provides transmission diversity. Accordingly, compared to SISO systems, MIMO systems can achieve a greatly increased virtual aperture and leading to significant advantages, such as better detection performance, improved parameter identifiability, refined resolution, and direct applicability of adaptive array techniques [6].

The spatial diversity can be increased by the system with widely separated transmitter and receiver antennas. By this system, targets can be seen in different aspects, hence the information extracted by each matched filter only weakly correlated. As

a result, a better performance can be obtained [7]. In MIMO radar with colocated antennas, the transmission and reception arrays are closely spaced, therefore targets are relatively far away from the transmitter and receiver. In this case, the components extracted by matched filters contain the information of transmitting path from one of the transmitter antenna elements to one of the receiver antennas. Better spatial resolution can be achieved by using all the information of transmission paths [8].

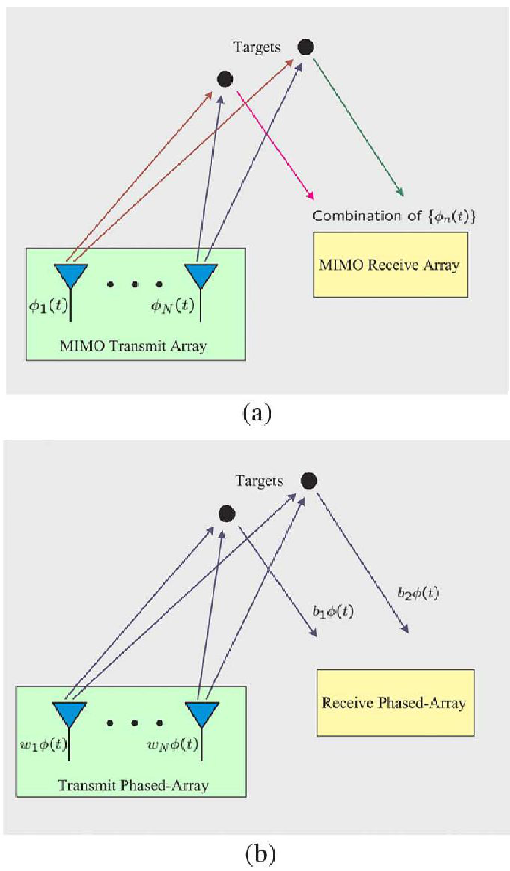

Figure 1.3: (a) MIMO radar system vs. (b) SIMO (phased array) radar system [4]

1.3 Signal Design in MIMO Radar

Following the introduction of MIMO radar a considerable effort has been dedicated to the design of the transmission signal and the synthesis of the waveform. Some approaches are carried out by maximizing the mutual information (MI) between the target impulse response and the reflected radar waveforms [9, 10]. Different methods [11, 12] aiming at matching given transmission beam patterns as well as minimizing the cross-correlation of reflected signals have been proposed. In particular, an algorithm to design a unimodulus signal set matching beam pattern specifications and suppressing sidelobes of both cross- and auto-correlations has been developed [13]. Instead of the beam pattern matching design [11, 12], [14], [6] present algorithms to synthesize waveform directly such that its covariance is close to a desired matrix $\boldsymbol{R}$, having good cross- and auto-correlation properties. Using different forms of weighting, the design problem was formulated as different mathematical expressions optimized under a constraint of low peak-to-average power ratio (PAR). Several computational efficient Cyclic Algorithms (CA) were presented to design unimodular MIMO waveforms minimizing the distance between the covariance matrix and a desired matrix.
Ambiguity function is a two dimensional function with time-delay and Doppler shift and it describes the interferrence due to receiver matched filter returned signals. As ambiguity function of transmitted waveform exploring the range and Doppler resolution, considering the joint estimation of time delay and Doppler shift in a SISO radar system, [15] optimum waveform is designed by minimizing estimation error. To obtain the optimum waveform,the efficient method approxiamate the convex design region by a polygon. In MIMO radar system, [16] proposes an algorithm to reduces the sidelobes of ambiguity function of transmitted waveform and makes the energy

of ambiguity function spread evenly in the range and angular dimensions.

1.4 Contribution of this thesis

In the methods mentioned in Section 1.3 above, the designs are carried out by minimizing the difference between the desired and the actual covariance matrices in terms of the commonly used Euclidean distance (ED), which in matrix computations, is also often known as the Frobenius distance (FD). Being positive semi-definite (PSD) and Hermitian symmetric, the PSD matrices are structurally constrained and thus form a *manifold* $\mathcal{M}$ in the complex linear vector space $\mathcal{H}$ of all $M \times M$ matrices [17]. Therefore, the commonly used ED may not be appropriate for measuring the distance between two PSD matrices; rather, we should measure the distance along the surface of the manifold. This concept is akin to finding the distance between two cities on earth: The ED between two cities is neither informative nor accurate. By the same reasoning, we suggest that the discrepancy between two of these matrices is more accurately measured along the surface of the PSD manifold. Thus in this thesis, we formulate the problem of designing the radar transmission signal having a covariance matrix close to a desired matrix, the distance between the two matrices being measured in terms of a metric suitable for measuring on a manifold – the Riemannian distance (RD).

In addition, we also aim to suppress the sidelobes of ambiguity functions where ambiguity function is a two dimensional function with parameters time delay and Doppler shift describing the interference caused by receiver matched filter returned signals [16]. Each waveform is described as a linear combination of a set of orthonormal functions. We minimimize the distance between the covariance of transmitted

signals and a desired covariance and constraint on sidelobes of ambiguity functions. In our design, we also consider the constraint on the bandwidth of the signal. In this thesis, we develop an algorithm to approximate the original non-convex quartic problem by a convex quadratic problem and solve it iteratively. The optimization using RD as the measure shows much faster convergence compared to the corresponding problem measured in ED. It also yields signal designs having better accuracy in estimating the location and velocity of the targets.

As WLJ basis is an orthonormal set with optimum time-bandwidth product, WLJ functions have a narrow essential bandwidth. In our design, we found that the use of WLJ basis [1] will yield signals with best time-frequency requirement.

1.5 Outline of the Thesis

In this thesis, we propose an algorithm to design transmitted signals by minimizing the distance between covariance of signal vectors and desired covariance while keeping sidelobes of ambiguity functions to be small using both ED and RD metrics. In Chapter 1, we have introduced MIMO radar systems and presented a brief review of some existing researches on the topic of MIMO radar signal design. In Chapter 2, we argue that the error between covaraince of signal vectors and desired covariance should be measured on the manifold of Hermitian-sysmmetric positive semi-definite matrices and formulate the optimization using the Riemannian distance metric. Next, according to the difficulty of solving a non-convex optimization, Jia Xu developped an effective iterative algorithm based on successive approximation of the non-convex quartic problem by a convex quadratic problem [18]. That algorithm was developed in the context of a different MIMO radar signal design problem, and in this thesis we will

adapt that algorithm to the problem. Furthermore we will show how the parameters of the algorithm can be chosen and we will provide an explanation for the good convergence behavior un the RD case. Considering interference in frequency domain, in Chapter 4, we complete the MIMO radar signal design by adding a frequency bandwidth constraint. Numerical experiments are shown in Chapter 5. Finally, the conclusion of the thesis and our future work are presented in Chapter 6.

Chapter 2

Signal Design in MIMO Radar using Euclidean and Riemannian Distances

Several techniques for MIMO radar waveform design are based on minimizing the distance between covariance matrix and a desired covariance matrix (which is usually a scaled identity matrix) [14, 6]. In these papers, they measure the distance between the matrices using the Frobenius distance/Euclidean distance (ED), which is the length of the shortest path between two matrices in the ambient space. In this chapter, we synthesize transmitted signals to match a desired covariance matrix while controling the sidelobes of the ambiguity function to be small. Different from the existing literature, we minimize the distance between the covariance matrix of the synthesized signal and the desired covariance matrix using a Riemannian distance (RD) on the manifold of symmetrical positive semi-definite matrices.

2.1 MIMO Signal Model

We consider a MIMO radar system equipped with M transmitter antennas and M receiver antennas. The signal to be transmitted from m^{th} antenna $x_m(t)$ is a linear combination of $K \geq M$ orthogonal unit-energy functions $s_k(t)$ such that

$$\begin{aligned} x_m(t) &= \sum_{k=1}^{K} \alpha_{mk} s_k(t) \\ &= \boldsymbol{\alpha}_m^T \cdot \boldsymbol{s}(t), \end{aligned} \tag{2.1}$$

where K denotes the number of orthonormal functions $\{s_k(t)\}_{k=1}^{K}$. The real coefficient vector associated with the mth transmission is

$$\boldsymbol{\alpha}_m = \begin{bmatrix} \alpha_{m1} \\ \alpha_{m2} \\ \vdots \\ \alpha_{mK} \end{bmatrix}. \tag{2.2}$$

The orthonormal functions can be represented in a vector by

$$\boldsymbol{s}(t) = \begin{bmatrix} s_1(t) \\ s_2(t) \\ \vdots \\ s_K(t) \end{bmatrix} \tag{2.3}$$

The transmitted signal can be then expressed as $\boldsymbol{x}(t)$ be

$$\boldsymbol{x}(t) = \begin{bmatrix} x_1(t) \\ x_2(t) \\ \vdots \\ x_M(t) \end{bmatrix}. \tag{2.4}$$

Let matrix $\boldsymbol{A}$ denote the matrix

$$\boldsymbol{A} = \begin{bmatrix} \boldsymbol{\alpha}_1 & \boldsymbol{\alpha}_2 & \dots & \boldsymbol{\alpha}_K \end{bmatrix}^T \in \mathbb{C}^{M \times K}. \tag{2.5}$$

The transmitted signals can be written as

$$\boldsymbol{x}(t) = \boldsymbol{A}\boldsymbol{s}(t). \tag{2.6}$$

In this thesis, we consider joint estimation of both the location and the velocity of the target. The distance of target away from the antenna array can be estimated by the time delay of the returned signal. The target velocity can be analyzed using the Doppler shift. If a target has a constant radial velocity v_t, the shift in the carrier frequency is called the *Doppler shift* ν [2]

$$\nu \triangleq f_c \left(\frac{2v_t}{c} \right), \tag{2.7}$$

where f_c is carrier frequency and c is the speed of light. The value of the ambiguity function for a particular pair $(\tau, \nu)$is the time response of a filter matched to a given finite energy signal when the signal is received with a time delay τ and a Doppler

shift ν. The ambiguity function of any arbitrary pair of transmitted signals is

$$f_{m_1 m_2}(\tau, \nu) = \int x_{m_1}(t) x^*_{m_2}(t+\tau) e^{j2\pi\nu t} dt. \tag{2.8}$$

Since

$$x_{m_1}(t) = \sum_{k=1}^{K} \alpha_{m_1 k} s_k(t), \text{ with } 1 \leq k \leq K, \tag{2.9a}$$

$$x_{m_2}(t+\tau) = \sum_{k=1}^{K} \alpha_{m_2 k} s_k(t+\tau), \text{ with } 1 \leq k \leq K, \tag{2.9b}$$

we have

$$\begin{aligned} f_{m_1 m_2}(\tau, \nu) &= \int x_{m_1}(t) x^*_{m_2}(t+\tau) e^{j2\pi\nu t} dt \\ &= \sum_{i=1}^{K} \sum_{j=1}^{K} \int \alpha_{m_1 i} s_i(t) \alpha^*_{m_2 j} s^*_j(t+\tau) e^{j2\pi\nu t} dt \\ &= \sum_{i=1}^{K} \sum_{j=1}^{K} \alpha_{m_1 i} \alpha^*_{m_2 j} \int s_i(t) s^*_j(t+\tau) e^{j2\pi\nu t} dt. \end{aligned} \tag{2.10}$$

If we let $\phi_{ij}(\tau, \nu)$ denote the ambiguity function for $s_i(t)$ and $s_j(t)$

$$\phi_{ij}(\tau, \nu) = \int s_i(t) s^*_j(t+\tau) e^{j2\pi\nu t} dt, \tag{2.11}$$

and if we define the ambiguity matrix for $\boldsymbol{s}(t)$ as the matrix $\boldsymbol{\Phi}(\tau, \nu)$ where the $(i, j)^{th}$ element is $\phi_{ij}(\tau, \nu)$, then the complex ambiguity matrix for $\boldsymbol{x}(t)$ can be written as

$$\boldsymbol{F}(\tau, \nu) = \boldsymbol{A} \boldsymbol{\Phi}(\tau, \nu) \boldsymbol{A}^H. \tag{2.12}$$

For further reference, we observe that since the signals in $\boldsymbol{s}(t)$ are orthonormal, $\boldsymbol{\Phi}(0,0) = \boldsymbol{I}$, and hence $\boldsymbol{F}(0,0) = \boldsymbol{A}\boldsymbol{A}^H$.

2.2 Introduction to Euclidean and Riemannian Distances

The objective of proposed design is to minimize the error between the covariance matrix of the designed signals and a desired covariance. In other words, we want the distance between the achieved covariance and the specified covariance to be small. The distance between two positive semi-definite (PSD) symmetric matrices $d(\boldsymbol{P}_1, \boldsymbol{P}_2)$ can be measured in various ways. The most commonly used is the *Euclidean distance* (ED)

$$\begin{aligned} d_E(\boldsymbol{P}_1, \boldsymbol{P}_2) &= \|\boldsymbol{P}_1 - \boldsymbol{P}_2\|_F \\ &= \sqrt{\mathrm{tr}\big((\boldsymbol{P}_1 - \boldsymbol{P}_2)(\boldsymbol{P}_1 - \boldsymbol{P}_2)^H\big)} \end{aligned} \tag{2.13}$$

The Euclidean distance implicitly treats $\boldsymbol{P}_1$ and $\boldsymbol{P}_2$ as elements of the ambient space (of complex $M \times M$ matrices) and it measures the length of the shortest path from $\boldsymbol{P}_2$ to $\boldsymbol{P}_1$ in that space — a path that may include matrices that are not PSD. We argue that it is inappropriate to model the mismatch by ED as a covariance matrix is not free-structured, but positive semi-definite (PSD) and symmetric. An alternative is to recognize that the set of PSD matrices forms a Riemannian manifold in the ambient space. It can be argued that it is more appropriate to measure the distance between $\boldsymbol{P}_1$ and $\boldsymbol{P}_2$ on that manifold $\mathcal{M}$. According to the special structure, the matrices form a hyper-surface called a *manifold* in signal space. Therefore the distance between two

matrices should be the length of the path which along the surface of the manifold between two matrices. The length of the path between two points on the manifold $\mathcal{M}$ is given by [19, 20]

$$\ell(\boldsymbol{P}) = \int_{\theta_1}^{\theta_2} g_{\boldsymbol{P}}^{1/2}(\dot{\boldsymbol{P}}, \dot{\boldsymbol{P}}) d\theta \tag{2.14}$$

where $\dot{\boldsymbol{P}} = \frac{\boldsymbol{P}}{d\theta}$ and $g_{\boldsymbol{P}}^{1/2}(\dot{\boldsymbol{P}}, \dot{\boldsymbol{P}})$ is an inner product metrics, called a *Riemannian metric*, at $\boldsymbol{P}$ on the manifold $\mathcal{M}$, which can be define in various ways. The curve of minimum length on the manifold linking two PSD matrices $\boldsymbol{P}_1$ and $\boldsymbol{P}_2$ is called a *geodesic* and the length of the geodesic is called the *Riemannian distance* (RD) between the two points, i.e.,

$$d_R(\boldsymbol{P}_1, \boldsymbol{P}_2) \triangleq \min_{\boldsymbol{P}:[\theta_1,\theta_2]\to\mathcal{M}} \{\ell(\boldsymbol{P})\} \tag{2.15}$$

It is difficult to evaluate the RD directly from (2.15. Therefore we use the following concept [17] to determine RD. Let $\mathcal{H}$ denote the Euclidean space of matrices. Here we set up a mapping π: $\mathcal{M} \to \mathcal{H}$ such that $\boldsymbol{P} = \tilde{\boldsymbol{P}}\tilde{\boldsymbol{P}}^H$ where $\tilde{\boldsymbol{P}} \in \mathcal{H}$, $\boldsymbol{P} \in \mathcal{M}$. By choosing the mapping π, we can find a Euclidean subspace $\mathcal{U}_{\mathcal{H}}$ at $\tilde{\boldsymbol{P}}$ of $\mathcal{H}$ which is *isometric* with $\mathcal{T}_{\mathcal{M}}(\boldsymbol{P})$, the tangent space at $\boldsymbol{P}$ in the manifold $\mathcal{M}$, i.e., the geodesic between $\boldsymbol{P}_1, \boldsymbol{P}_2 \in \mathcal{M}$ can be *lifted* to $\tilde{\boldsymbol{P}}_1, \tilde{\boldsymbol{P}}_2 \in \mathcal{U}_{\mathcal{H}}$. Therefore, the RD on the manifold can be expressed directly in Euclidean space $\mathcal{U}_{\mathcal{H}}$ in which ED is the measure distance. If we consider the mapping $\tilde{\boldsymbol{P}}\tilde{\boldsymbol{P}}^H = \boldsymbol{P}$, i.e., $\tilde{\boldsymbol{P}} = \boldsymbol{P}^{1/2}\boldsymbol{U}$, where $\tilde{\boldsymbol{P}} \in \mathcal{H}$, $\boldsymbol{P} \in \mathcal{M}$, and $\boldsymbol{U}$ is a unitary matrix. The RD between $\boldsymbol{P}_1$ and $\boldsymbol{P}_2$ is given by

$$\begin{aligned} d_{R_1}(\boldsymbol{P}_1, \boldsymbol{P}_2) &= \sqrt{\mathrm{tr}\boldsymbol{P}_1 + \mathrm{tr}\boldsymbol{P}_2 - 2\mathrm{tr}\big(\boldsymbol{P}_1^{1/2}\boldsymbol{P}_1\boldsymbol{P}_2^{1/2}\big)} \\ &= \sqrt{\mathrm{tr}\boldsymbol{P}_1 + \mathrm{tr}\boldsymbol{P}_2 - 2\mathrm{tr}\big(\boldsymbol{P}_1\boldsymbol{P}_2\big)^{1/2}} \end{aligned} \tag{2.16}$$

If we use the mapping $\tilde{\boldsymbol{P}}^{1/2}\tilde{\boldsymbol{P}}^{1/2} = \boldsymbol{P}$ by choosing the unitary matrix to be identity, then the RD between $\boldsymbol{P}_1$ and $\boldsymbol{P}_2$ can be written as

$$\begin{aligned} d_{R_2}(\boldsymbol{P}_1, \boldsymbol{P}_2) &= \sqrt{\mathrm{tr}\boldsymbol{P}_1 + \mathrm{tr}\boldsymbol{P}_2 - 2\mathrm{tr}\big(\boldsymbol{P}_1^{1/2}\boldsymbol{P}_2^{1/2}\big)} \\ &= \sqrt{\mathrm{tr}\big((\boldsymbol{P}_1^{1/2} - \boldsymbol{P}_2^{1/2})(\boldsymbol{P}_1^{1/2} - \boldsymbol{P}_2^{1/2})^H\big)} \\ &= \left\|\boldsymbol{P}_1^{1/2} - \boldsymbol{P}_2^{1/2}\right\|_F^2 \end{aligned} \tag{2.17}$$

2.3 Optimization Formulation in ED and RD

In single antenna radar, typically we seek to design a waveform that results in sidelobes are small with respect to the power of the waveform; i.e., $|f_{1,1}(\tau,\nu)| \ll f_{1,1}(0,0)$ for all τ and ν that are not close to zero [2, 15]. The principles of MIMO radar signal design are similar, although since $\boldsymbol{x}(t)$ is now a vector, there is an additional degree of design freedom namely the spatial covariance matrix $\boldsymbol{F}(0,0)$. In isotropic applications the desired covariance matrix would typically be a scaled identity matrix, but there are other applications in which other spatial covariances would be appropriate. We will denote the desired covariance by $\boldsymbol{R}_d$. To exert control over the sidelobes, we could consider imposing element-wise constraints of the form $|f_{m_1,m_2}(\tau,\nu)| \leq \epsilon_{m_1,m_2}(\tau,\nu)$ for each pair of (m_1, m_2) with $m_1 \geq m_2$ and suitably sampled values for τ and ν. An alternative that significantly reduces the computational cost at the price of somewhat more coarse control over the sidelobes is to impose norm constraints of the form $\|\boldsymbol{F}(\tau,\nu)\|_F^2 \leq \epsilon(\tau,\nu)$, again for suitably sampled values for τ and ν. With those sidelobe constraints, a desired covariance $\boldsymbol{R}_d$ and an energy constraint $\mathrm{tr}\big(\boldsymbol{A}\boldsymbol{A}^H\big) \leq \mathrm{tr}(\boldsymbol{R}_d)$, the design problem can be formulated as

$$\begin{aligned} \underset{\boldsymbol{A}}{\text{minimize}} \quad & d^2\left(\boldsymbol{A}\boldsymbol{A}^H, \boldsymbol{R_d}\right) \\ \text{subject to} \quad & \left\|\boldsymbol{A}\boldsymbol{\Phi}(\tau_{\ell_1}, \nu_{\ell_2})\boldsymbol{A}^H\right\|_F^2 \leq \epsilon(\tau_{\ell_1}, v_{\ell_2}),\ \ell_1, \ell_2 = 1, 2, \ldots, L \\ & \text{tr}(\boldsymbol{A}\boldsymbol{A}^H) \leq \text{tr}(\boldsymbol{R}_d), \end{aligned} \tag{2.18}$$

where we have chosen L pairs (τ_ℓ, ν_ℓ) at which to impose the sidelobe constraints, and $d(\cdot\ ,\ \cdot)$ is either

$$d_E(\boldsymbol{A}\boldsymbol{A}^H, \boldsymbol{R}_d) = \left\|\boldsymbol{A}\boldsymbol{A}^H - \boldsymbol{R_d}\right\|_F \tag{2.19}$$

or

$$d_{R_2}(\boldsymbol{A}\boldsymbol{A}^H, \boldsymbol{R}_d) = \left\|\left(\boldsymbol{A}\boldsymbol{A}^H\right)^{1/2} - \boldsymbol{R_d}^{1/2}\right\|_F \tag{2.20}$$

In general, $d_{R_1} \neq d_{R_2}$, as the expressions are not equal. They are equal only when the last terms in each expression are equal; i.e.,

$$\text{tr}\left(\left(\boldsymbol{P}_1\boldsymbol{P}_2\right)^{1/2}\right) = \text{tr}\left(\boldsymbol{P}_1^{1/2}\boldsymbol{P}_2^{1/2}\right). \tag{2.21}$$

If we choose $\boldsymbol{R}_d$ to be the identity matrix, then $d_{R_1}(\boldsymbol{A}\boldsymbol{A}^H, \boldsymbol{R}_d) = d_{R_2}(\boldsymbol{A}\boldsymbol{A}^H, \boldsymbol{R}_d)$. Therefore, in the rest of this thesis, we use d_{R_2} to represent the Riemannian distance measurement, because of its simplicity [21]. Note, the first arguement in (2.18) can be written in both ED and RD as $d_{(E/R)}\left(\boldsymbol{A}\boldsymbol{\Phi}(\tau_{\ell_1}, \nu_{\ell_2})\boldsymbol{A}^H(\boldsymbol{A}\boldsymbol{\Phi}\left(\tau_{\ell_1}, \nu_{\ell_2}\right)\boldsymbol{A}^H\right)^H, \boldsymbol{0}\right) \leq \epsilon(\tau_{\ell_1}, v_{\ell_2}),\ \ell_1, \ell_2 = 1, 2, \ldots, L$.

Becaues the expressions in ED and RD are the same, we formulate the first argument

in ED. Optimization using the Euclidean distance method can be written as

$$\begin{aligned} \underset{\boldsymbol{A}}{\text{minimize}} \quad & \left\|\boldsymbol{A}\boldsymbol{A}^H - \boldsymbol{R_d}\right\|_F^2 \\ \text{subject to} \quad & \left\|\boldsymbol{A}\boldsymbol{\Phi}(\tau_{\ell_1}, \nu_{\ell_2})\boldsymbol{A}^H\right\|_F^2 \leq \epsilon(\tau_{\ell_1}, \upsilon_{\ell_2}),\ \ell_1, \ell_2 = 1, 2, \ldots, L \\ & \text{tr}(\boldsymbol{A}\boldsymbol{A}^H) \leq \text{tr}(\boldsymbol{R}_d) \end{aligned} \tag{2.22}$$

If $\boldsymbol{A} = \boldsymbol{U}\boldsymbol{\Sigma}\boldsymbol{V}^H$ denotes the singular value decomposition of $\boldsymbol{A}$, then we can write

$$\left(\boldsymbol{A}\boldsymbol{A}^H\right)^{1/2} = \boldsymbol{A}\boldsymbol{V}\boldsymbol{U}^H. \tag{2.23}$$

The proof of (2.23) is as follows:

Proof. Perform a compact singular value decomposition on $\boldsymbol{A}$

$$\boldsymbol{A} = \boldsymbol{U}\boldsymbol{\Sigma}\boldsymbol{V}^H \tag{2.24}$$

where $\boldsymbol{U}$ and $\boldsymbol{V}$ are left and right singular vectors of $\boldsymbol{A}$. We can write

$$\begin{aligned} \left(\boldsymbol{A}\boldsymbol{A}^H\right)^{1/2} &= \left(\boldsymbol{U}\boldsymbol{\Sigma}\boldsymbol{V}^H\boldsymbol{V}\boldsymbol{\Sigma}^H\boldsymbol{U}^H\right)^{1/2} \\ &= \left(\boldsymbol{U}\boldsymbol{\Sigma}\boldsymbol{I}_M\boldsymbol{\Sigma}^H\boldsymbol{U}^H\right)^{1/2} \\ &= \boldsymbol{U}\left(\boldsymbol{\Sigma}\boldsymbol{\Sigma}^H\right)^{1/2}\boldsymbol{U}^H \\ &= \boldsymbol{U}\boldsymbol{\Sigma}\boldsymbol{U}^H. \end{aligned} \tag{2.25}$$

Multiplying (2.24) by $\boldsymbol{V}$ on both sides, we have

$$\boldsymbol{A}\boldsymbol{V} = \boldsymbol{U}\boldsymbol{\Sigma}\boldsymbol{V}^H\boldsymbol{V} = \boldsymbol{U}\boldsymbol{\Sigma} \tag{2.26}$$

Subsitituting (2.26) into (2.25), we have $\left(\boldsymbol{A}\boldsymbol{A}^H\right)^{1/2} = \boldsymbol{A}\boldsymbol{V}\boldsymbol{U}^H$ [21]. □

According to (2.23), the optimization problem using the Riemannian distance method can be rewritten as

$$\begin{aligned} \underset{\boldsymbol{A}}{\text{minimize}} \quad & \left\| \boldsymbol{A}\boldsymbol{V}\boldsymbol{U}^H - \left(\boldsymbol{R_d}\right)^{1/2} \right\|_F^2 \\ \text{subject to} \quad & \left\| \boldsymbol{A}\boldsymbol{\Phi}(\tau_{\ell_1}, \nu_{\ell_2})\boldsymbol{A}^H \right\|_F^2 \leq \epsilon(\tau_{\ell_1}, \upsilon_{\ell_2}),\ \ell_1, \ell_2 = 1, 2, \ldots, L \\ & \text{tr}(\boldsymbol{A}\boldsymbol{A}^H) \leq \text{tr}(\boldsymbol{R}_d). \end{aligned} \tag{2.27}$$

2.4 An Iterative Algorithm

The problem in (2.18) is not convex, due to the quartic structure of the sidelobe constraints and the nature of the objective. While that makes it difficult to find a globally optimal solution, we will develope an effective iterative algorithm based on successive approximation of the problem by a convex quadratic optimzation problem. In particular, at the nth iteration of the algorithm we will replace one of $\boldsymbol{A}^{(n)}$ in the objective and in each constraint with $\boldsymbol{A}^{(n-1)}$ and we will solve the resulting convex quadratic problem for an intermediate solution $\breve{\boldsymbol{A}}^{(n)}$. Then we generate the nth iterate $\boldsymbol{A}^{(n)}$ using $\boldsymbol{A}^{(n)} = \breve{\boldsymbol{A}}^{(n)} + \gamma^{(n)}\left(\boldsymbol{A}^{(n-1)} - \breve{\boldsymbol{A}}^{(n)}\right)$, where $\gamma^{(n)}$ controls the step size of the algorithm [18]. At a particular point, the convex approximation may not be the best suitable. As a result, the intermediate solution may be dragged far away from the optimum. Therefore, we update $\boldsymbol{A}^{(n)}$ based on the previous $\boldsymbol{A}^{(n-1)}$. The problem

to be solved at each iteration takes the form

$$\begin{aligned} \underset{\breve{\boldsymbol{A}}^{(n)}}{\text{minimize}} \quad & d^2\left(\breve{\boldsymbol{A}}^{(n)}\boldsymbol{A}^{(n-1)^H}, \boldsymbol{R}_d\right) \\ \text{subject to} \quad & \left\|\breve{\boldsymbol{A}}^{(n)}\boldsymbol{\Phi}(\tau_{\ell_1}, \nu_{\ell_2})\boldsymbol{A}^{(n-1)^H}\right\|_2^2 \leq \epsilon(\tau_{\ell_1}, \nu_{\ell_2}),\ \ell_1, \ell_2 = 1, 2, \ldots, L \\ & \text{tr}\left(\breve{\boldsymbol{A}}^{(n)}\boldsymbol{A}^{(n-1)^H}\right) \leq \text{tr}(\boldsymbol{R}_d) \end{aligned} \tag{2.28}$$

In the case of the Euclidean distance, the objective function in (2.28) can be written as

$$d_E^2\left(\breve{\boldsymbol{A}}^{(n)}\boldsymbol{A}^{(n-1)^H}, \boldsymbol{R}_d\right) = \left\|\breve{\boldsymbol{A}}^{(n)}\boldsymbol{A}^{(n-1)^H} - \boldsymbol{R_d}\right\|_F^2. \tag{2.29}$$

In the case of the Riemannian distance, if $\boldsymbol{A}^{(n-1)} = \boldsymbol{U}^{(n-1)}\boldsymbol{\Sigma}^{(n-1)}\boldsymbol{V}^{(n-1)^H}$ denotes the compact SVD of $\boldsymbol{A}^{(n-1)}$, the objective can be written as

$$d_{R_2}^2\left(\breve{\boldsymbol{A}}^{(n)}\boldsymbol{A}^{(n-1)^H}, \boldsymbol{R}_d\right) = \left\|\breve{\boldsymbol{A}}^{(n)}\boldsymbol{V}^{(n-1)}\boldsymbol{U}^{(n-1)^H} - \boldsymbol{R}_d^{1/2}\right\|_F^2. \tag{2.30}$$

Since both $d_E^2\left(\breve{\boldsymbol{A}}^{(n)}\boldsymbol{A}^{(n-1)^H}, \boldsymbol{R}_d\right)$ and $d_{R_2}^2\left(\breve{\boldsymbol{A}}^{(n)}\boldsymbol{A}^{(n-1)^H}, \boldsymbol{R}_d\right)$ are convex quadratic functions of $\breve{\boldsymbol{A}}^{(n)}$ and the constraints in (2.28) are also convex quadratic and linear in $\breve{\boldsymbol{A}}^{(n)}$, repectively, the problem in (2.28) is convex and can be efficiently solved [21]. Thus we obtain the iterative algorithm in Table 2.1. The optimization in each iteration can be solved by the standard optimization tools such as CVX [22].

Table 2.1: Iterative Algorithm [21]

Step 0	Select an initial matrix $\boldsymbol{A}^{(0)}$. Select a. Set $\gamma^{(0)} = 1$, $n = 0$.
Step 1	Update iteration index $n \leftarrow n + 1$
Step 2	In RD case only, perform an SVD of $\boldsymbol{A}^{(n-1)}$ to obtain $\boldsymbol{U}^{(n-1)}$ and $\boldsymbol{V}^{(n-1)}$
Step 3	Given $\boldsymbol{A}^{(n-1)}$, and $\left(\boldsymbol{U}^{(n-1)} \text{ and } \boldsymbol{V}^{(n-1)}\right)$ solve the convex quadratic program in (2.28) to obtain $\breve{\boldsymbol{A}}^{(n)}$
Step 4	Compute the step size $\gamma^{(n)} = \gamma^{(n-1)}(1 - a\gamma^{(n-1)})$
Step 5	Update $\boldsymbol{A}^{(n)}$ using $\boldsymbol{A}^{(n)} = \breve{\boldsymbol{A}}^{(n)} + \gamma^{(n)}\left(\boldsymbol{A}^{(n-1)} - \breve{\boldsymbol{A}}^{(n)}\right)$
Step 6	Test for convergence and if the test fails return to Step 1

2.5 Objective Functions in RD and ED Methods

As we want to minimize the interferrence between any two transmitted signals, we set $\boldsymbol{R}_d = \boldsymbol{I}$. The objective functions of the ED and RD optimization problems (2.29), (2.30) can be written as,

$$\underset{\breve{\boldsymbol{A}}^{(n)}}{\text{minimize}} \quad \left\| \breve{\boldsymbol{A}}^{(n)} \boldsymbol{U}^{(n-1)} \boldsymbol{\Sigma}^{(n-1)} \boldsymbol{V}^{(n-1)^H} - \boldsymbol{I} \right\|_F^2, \tag{2.31}$$

$$\underset{\breve{\boldsymbol{A}}^{(n)}}{\text{minimize}} \quad \left\| \breve{\boldsymbol{A}}^{(n)} \boldsymbol{V}^{(n-1)} \boldsymbol{I} \boldsymbol{U}^{(n-1)^H} - \boldsymbol{I} \right\|_F^2. \tag{2.32}$$

It can be seen that $\left(\boldsymbol{U}^{(n-1)} \boldsymbol{\Sigma}^{(n-1)} \boldsymbol{V}^{(n-1)^H}\right)$ in Eq. (2.31) is a general matrix that is not necessarily unitary, whereas $\left(\boldsymbol{V}^{(n-1)} \boldsymbol{I} \boldsymbol{U}^{(n-1)^H}\right)$ in Eq. (2.32) is always unitary. As it is desired to minimize the difference between the design covariance matrix and $\boldsymbol{I}$, then the matrix $\breve{\boldsymbol{A}}^{(n)}$ should be close to unitary. Hence in the search of $\breve{\boldsymbol{A}}^{(n)}$ under RD, the search space will be constrained to a relevant space that is smaller than the

more general space in the case of searching under ED.

If we replace the $\boldsymbol{\Sigma}$ in (2.31) by an identity matrix,

$$\underset{\breve{\boldsymbol{A}}^{(n)}}{\text{minimize}} \quad \left\| \breve{\boldsymbol{A}}^{(n)} \boldsymbol{U}^{(n-1)} \boldsymbol{I}^{(n-1)} \boldsymbol{V}^{(n-1)^H} - \boldsymbol{I} \right\|_F^2, \tag{2.33}$$

the optimization problem has similar convergence rate by using (2.32) and (2.33). Therefore, the scaling of the singular value matrix has dominant effect on convergence rate.

Chapter 3

Bandwidth Consideration in Design

If the orthonormal functions have finite time duration, the design of the signal $x_m(t)$ in previous section has finite time duration but has no specific bandwidth limitation. In practice, we may require to design signals which is finite in both time duration and in *essential* bandwidth. Here, we take into consideration the bandwidth constraint and other issues.

3.1 Bandwidth Constraint

In order to avoid interference in frequency domain, we aim to synthesize a transmitted signal that has a small essential bandwidth. Hence we add a bandwidth constraint to previous optimization. We impose the constraint that the magnitude of the Fourier transform of $x_m(t)$, which is $|X_m(f)|$, has to be small if $f < f_0$. According to the

linerarity property of Fourier transform that

$$\mathcal{F}[ax(t) + by(t)] = a\mathcal{F}[x(t)] + b\mathcal{F}[y(t)] \tag{3.1}$$

the Fourier transform of $x_m(t)$ is

$$X_m(f) = \sum_{k=1}^{K} \alpha_{mk} S_k(f) \tag{3.2}$$

where $S_k(f)$ is the Fourier transform of $s_k(t)$. Therefore, the problem can be written as

$$\begin{aligned}
\underset{\breve{\boldsymbol{A}}^{(n)}}{\text{minimize}} \quad & d^2\left(\breve{\boldsymbol{A}}^{(n)}\boldsymbol{A}^{(n-1)^H}, \boldsymbol{R}_d\right) \\
\text{subject to} \quad & \left\|\breve{\boldsymbol{A}}^{(n)}\boldsymbol{\Phi}(\tau_{\ell_1}, \nu_{\ell_2})\boldsymbol{A}^{(n-1)^H}\right\|_F^2 \leq \epsilon(\tau_{\ell_1}, \nu_{\ell_2}),\ \ell_1, \ell_2 = 1, 2, \ldots, L \\
& \left|\sum_{k=1}^{K}[\breve{\boldsymbol{A}}^{(n)}]_{mk} S_k(f)\right|^2 \leq \Delta_f,\ 1 \leq m \leq M, f > f_0 \\
& \text{tr}\left(\breve{\boldsymbol{A}}^{(n)}\boldsymbol{A}^{(n-1)^H}\right) \leq \text{tr}(\boldsymbol{R}_d)
\end{aligned} \tag{3.3}$$

where f_0 is the constraint essential bandwidth and sample f suitably.

3.2 Seeking Minimum Bandwidth

In some practical situations, the signal bandwidth may be the most emphasized factor in the design. Under such circumstances, we may seek a signal that has the minimum bandwidth while keeping the covariance matrix error and the sidelobes low. Thus,

we may consider an alternate formulation

$$
\begin{aligned}
\underset{\breve{\boldsymbol{A}}^{(n)}}{\text{minimize}} \quad & f_0 \\
\text{subject to} \quad & \hat{d}^2\left(\breve{\boldsymbol{A}}^{(n)}\boldsymbol{A}^{(n-1)^H}, \boldsymbol{R}_d\right) \leq \varepsilon \\
& \left\|\breve{\boldsymbol{A}}^{(n)}\boldsymbol{\Phi}(\tau_{\ell_1}, \nu_{\ell_2})\boldsymbol{A}^{(n-1)^H}\right\|_F^2 \leq \epsilon(\tau_{\ell_1}, \nu_{\ell_2}),\ \ell_1, \ell_2 = 1, 2, \ldots, L \\
& \left|\sum_{k=1}^{K}[\breve{\boldsymbol{A}}^{(n)}]_{mk}S_k(f)\right|^2 \leq \Delta_f,\ 1 \leq m \leq M, f > f_0 \\
& \operatorname{tr}\left(\breve{\boldsymbol{A}}^{(n)}\boldsymbol{A}^{(n-1)^H}\right) \leq \operatorname{tr}(\boldsymbol{R}_d)
\end{aligned}
\tag{3.4}
$$

We use bisection search to find the minimum bandwidth f_0 which satisfy all the constraints.

Chapter 4

Selected Orthonormal Sets

Functions in an orthonormal set are mutually orthogonal and each function has unit energy. We examine the use of three real orthnormal basis functions $\{s_k(t)\}$ for the synthesis of the transmission signals: (i) Walsh functions, (ii) Cosine functions, and (iii) WLJ functions [1], a set of functions designed for optimal time-frequency concentration. In this chapter, we briefly review on three orthonormal sets.

4.1 Walsh Functions

The set of Walsh functions is a set of piecewise-constant functions that take on only two values, 1 and -1. For the time duration $[0, 1]$, the Walsh functions are defined by [23, 24, 25]

$$w_0(t) = 1; 0 \leq t \leq 1; \tag{4.1a}$$

$$w_1(t) = \begin{cases} 1 & ; 0 \leq t \leq 1/2 \\ -1 & ; 1/2 \leq t \leq 1 \end{cases} \tag{4.1b}$$

$$w_{2_{(1)}}(t) = \begin{cases} 1 & ; 0 \leq t \leq 1/4, 3/4 \leq t \leq 1 \\ -1 & ; 1/4 \leq t \leq 3/4 \end{cases} \tag{4.1c}$$

$$w_{2_{(2)}}(t) = \begin{cases} 1 & ; 0 \leq t \leq 1/4, 1/2 \leq t \leq 3/4 \\ -1 & ; 1/4 \leq t \leq 1/2, 3/4 \leq t \leq 1 \end{cases} \tag{4.1d}$$

$$w_{k+1_{(2r-1)}}(t) = \begin{cases} w_{k_{(r)}}(2t) & ; 0 \leq t \leq 1/2 \\ (-1)^{r+1} w_{k_{(r)}}(2t-1) & ; 1/2 \leq t \leq 1 \end{cases} \tag{4.1e}$$

$$w_{k+1_{(2r)}}(t) = \begin{cases} w_{k_{(r)}}(2t) & ; 0 \leq t \leq 1/2 \\ (-1)^{r} w_{k_{(r)}}(2t-1) & ; 1/2 \leq t \leq 1 \end{cases} \tag{4.1f}$$

for $k = 1, 2, 3, \ldots$ and $r = 1, 2, 3, \ldots, 2^{m-1}$. Usually, the function $w_{k_{(1)}}$ is used, i.e.,

$$s_k^{Walsh}(t) = w_{k_{(1)}}(t) \tag{4.2}$$

This set has considerable practical advantage due to the piecewise constant nature of the functions which takes only two values. In addition, it is easy to generate with digital logic circuity. However, according to the "square-wave" structure, a Walsh function has a broad essential bandwidth.

4.2 Cosine Functions

For the time duartion $t \in [-1, +1]$, the cosine functions $\{\cos(2\pi kt); k = 0, \pm 1, \pm 2, \ldots\}$ are orthogonal. We only need to normalize the functions to provide an orthonormal

set. The cosine functions can be written as [25]

$$s_k^{\cos}(t) = \frac{1}{\sqrt{2}} \sum_{n=-k}^{k} \alpha_n \cos(2\pi nt) \tag{4.3}$$

with

$$\alpha_n = \frac{1}{\sqrt{2}} \int_{-1}^{1} s_k(t) \sin(2\pi nt) dt. \tag{4.4}$$

The cosine set has a sinusoidal structure and it is relatively easy to generate. Compare to Walsh function, cosine function has a narrower essential bandwidth.

4.3 WLJ Functions [1]

Given a continuous function $s(t)$ having finite energy, such that

$$\int_{-\infty}^{\infty} |s(t)|^2 dt = \int_{-\infty}^{\infty} |S(f)|^2 df < \infty, \tag{4.5}$$

let

$$E_T(s) \triangleq \frac{\int_{-T/2}^{T/2} |s(t)|^2 dt}{\int_{-\infty}^{\infty} |s(t)|^2 dt}, \tag{4.6a}$$

$$E_F(S) \triangleq \frac{\int_{-F}^{F} |S(f)|^2 dt}{\int_{-\infty}^{\infty} |S(f)|^2 dt}, \tag{4.6b}$$

where $S(f)$ is Fourier transform version of $s(t)$ and $E_T(s)$ and $E_F(S)$ are time and frequency energy concentration coefficients. The two parameters explicate the percentages of energy of the function $s(t)$ in the time duration $[-T/2, T/2]$ and frequency bandwidth $[-F, F]$. As $\int_{-T/2}^{T/2} |s(t)|^2 dt \leq \int_{-\infty}^{\infty} |s(t)|^2 dt$, it is clear that $0 \leq E_T(s) \leq 1$. analogously, for the frequency energy concentration coefficient we

have that $0 \leq E_F(S) \leq 1$. Ideally, we want the function $s(t)$ to have energy fully concentrated in both time and frequency regions $[-T/2, T/2]$ and $[-F, F]$, which means we have $E_T(s) = 1$ and $E_F(S) = 1$. However, due to the Fourier transform property [26] that a function can not be finite in both time domain and frequency domain simultaneously, that is impossible. Hence we seek to have the product of time and frequency energy concentration coefficients to be close to unity. Jin, Luo and Wong [1] showed that a linear combination of *prolate spheroidal wave* (PSW) function and its truncated version has maximum product of $E_T(s)$ and $E_F(S)$.

The PSW functions $\psi_k(t), k = 1, 2, \ldots$ are the set of eigenfunctions of (4.7), where the eigenfunction $\psi_k(t)$ is corresponing to k^{th} largest eigenvalue λ_k of (4.7). Given $T > 0$, $F > 0$

$$\int_{-T/2}^{T/2} \frac{\sin 2\pi F(t-\tau)}{\pi(t-\tau)} \psi(t) dt = \lambda \psi(t) \tag{4.7}$$

Let $D[\cdot]$ be a time-limiting operator defined by

$$D[s(t)] = \begin{cases} s(t) & t \in [-T/2, T/2] \\ 0 & \text{otherwise.} \end{cases} \tag{4.8}$$

The functions $D[\psi_k(t)]$ are orthogonal to each other. The following function (4.10) can achieve the maximum product of time and frequency energy concentration coefficients [1],

$$s_k^{WLJ}(t) = p_{1k}\psi_k(t) + q_{1k}D[\psi_k(t)] \tag{4.10}$$

The coefficients p_{1k} and q_{1k} in (4.10) can be calculated using

$$p_{1k} = \left(2 + 2\sqrt{\lambda_k}\right)^{-1/2} \qquad q_{1k} = \left(2\lambda_k + 2\lambda_k\sqrt{\lambda_k}\right)^{-1/2}. \tag{4.11}$$

The set of WLJ functions is an orthonormal set which has highy concentrated in both time and frequency.

In the following numerical experiments, we generate discrete prolate spheroidal sequences (DPSS). For each $k = 0, 1, \ldots, K-1$, the DPSS φ_k is defined as the real solution of

$$\sum_{m=0}^{K-1} \frac{\sin 2\pi F(n-m)}{\pi(n-m)} \varphi_k = \mu_k \varphi_k \tag{4.12}$$

Given

$$\rho_{mn} = \frac{\sin 2\pi F(n-m)}{\pi(n-m)}, \ m, n = 0, 1, \ldots, K-1 \tag{4.13}$$

Then μ_k and φ_k are also eigenvalues and eigenvectors of the matrix $\boldsymbol{\rho}$.

Chapter 5

Numerical Experiment

5.1 Optimization Results of Waveform Design using Walsh Functions, Cosine Functions and WLJ Functions

5.1.1 Time delay only

We consider the MIMO radar system having $M = 4$ transmitter antennas for which each transmission waveform is a linear combination of $K = 32$ Walsh functions as Figure 5.1. Each Walsh function is 64ms in duration and is illustrates in Figure 5.1. The ambiguity function has two parameters related to target which are time delay and Doppler shift. Time delay is the delay of returned signal which is related to distance between the target and the antenna array. The Doppler shift is a change in frequency which is related to the velocity of the target. If we consider time delay only, we fix $\nu = 0$ and relax the constraint which is the first constraint in (2.28)

by choosing $\epsilon(1,0) = 0.34M$ and $\epsilon(\tau,0) = 0.05M$ where $\tau > 1$. Here we suppress the sidelobes of the ambiguity functions of the transmitted signals to minimize the interference between a transmitted signal and its time or Doppler shifted version.

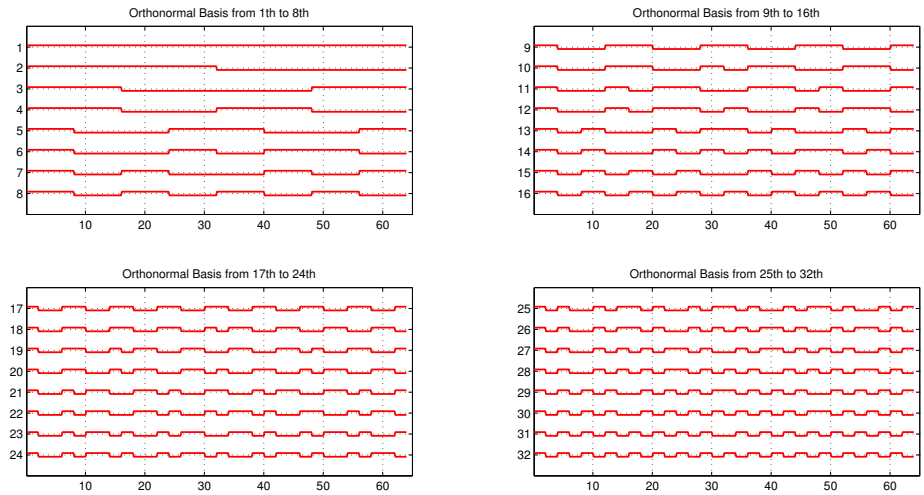

Figure 5.1: First 32 Walsh functions

We observe in Figure 5.2 that the error between signal covariance and the identity matrices converges to a low level by around 10 iterations for the design measured in RD. On the other hand, using ED to measure the matrix discrepancy takes around 150 iterations to reach similar level. The blue and green plots use ED measure, but compute the estimated error by RD and ED. The black and red lines use RD measure (Table 2.1) but compute the estimated error in terms of RD and ED respectively.

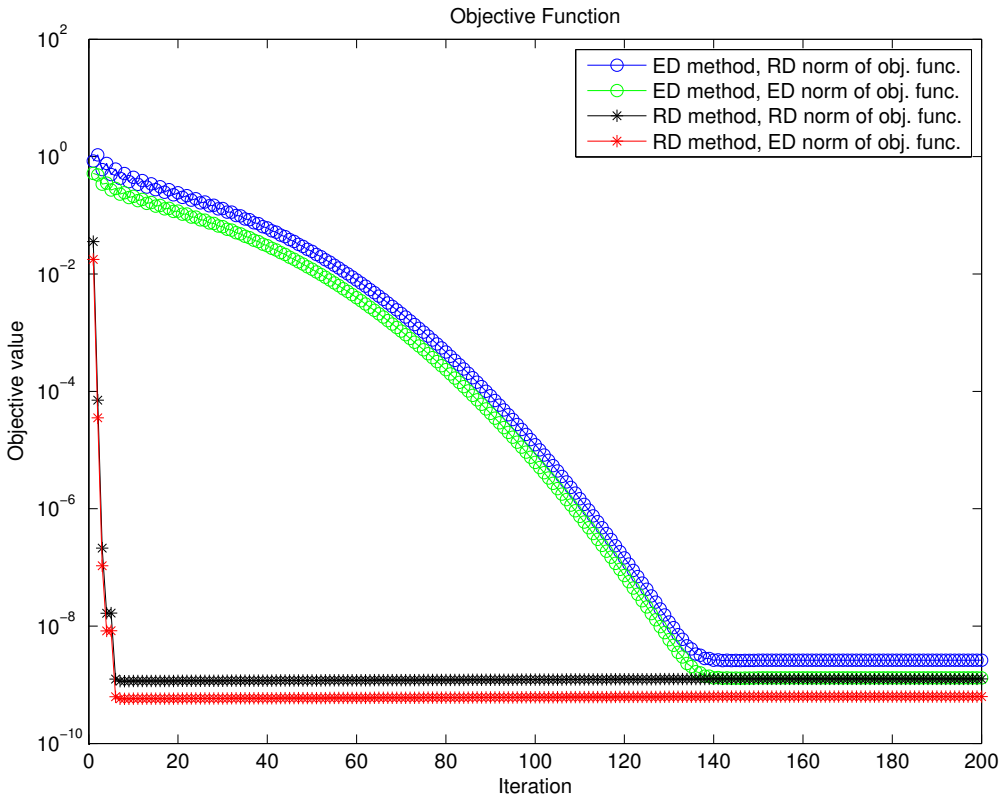

Figure 5.2: Error convergence using Walsh functions counting in iterations

It is observed that in each iteration, the design algorithm using RD as a measure has to perform an extra singular value decomposition (SVD). However, the advantage of fewer of iterations may outweight the additional cost per iteration, resulting in a much lower CPU time. Therefore, we instead of counting number in iterations, Figure 5.3 shows the convergence time (in terms of CPU time) of the design using both ED and RD as measures in the algorithm of Eqs. (2.28). The CPU time of each iteration measures the elapsed time of computation and expression transformation by CVX [22] in each iteration in unit of second. An Explanation of the faster convergence of

using the RD measure has been given in Section 2.5.

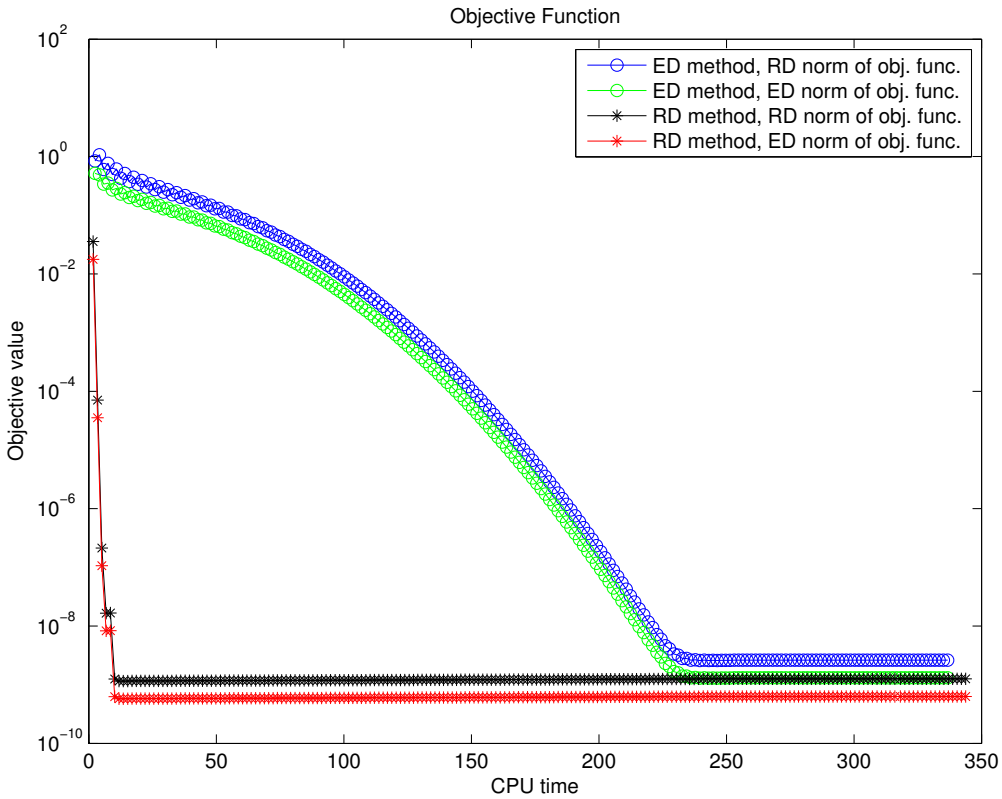

Figure 5.3: Error convergence using Walsh functions in length CPU time

Figure 5.4 illustrates the square norm of correlation with lag τ. The blue plot is the relaxed correlation constraint $\epsilon(\tau, 0)$. The red plot is the square norm of correlation with lag τ using RD measure. The green plot is the square norm of correlation with lag τ using ED measure.

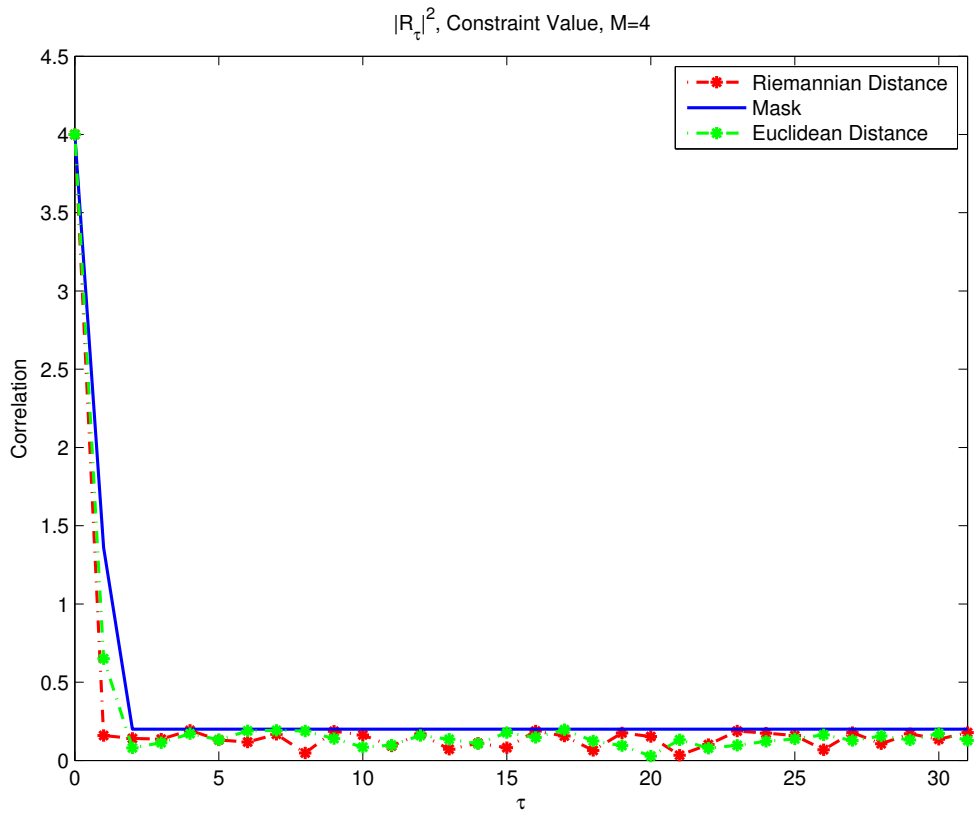

Figure 5.4: Correlation constraints, $\epsilon(1,0) = 0.34M$, $\epsilon(\tau,0) = 0.05M$, $M = 4$

If we want the covaraince to be close to identity, the solution of the coefficient matrix should be close to unitary. Therefore, we choose first M rows of normalized Hadamard matrix as starting point,

$$\boldsymbol{A}^{(0)} = \boldsymbol{H}(1:M,:), \tag{5.1}$$

where $\boldsymbol{H}$ is a $K \times K$ Hadamard matrix. At optimum the transmitted signals by RD measure is shown in Figure 5.5. Transmitted signals by ED measure is shown in

Figure 5.6.

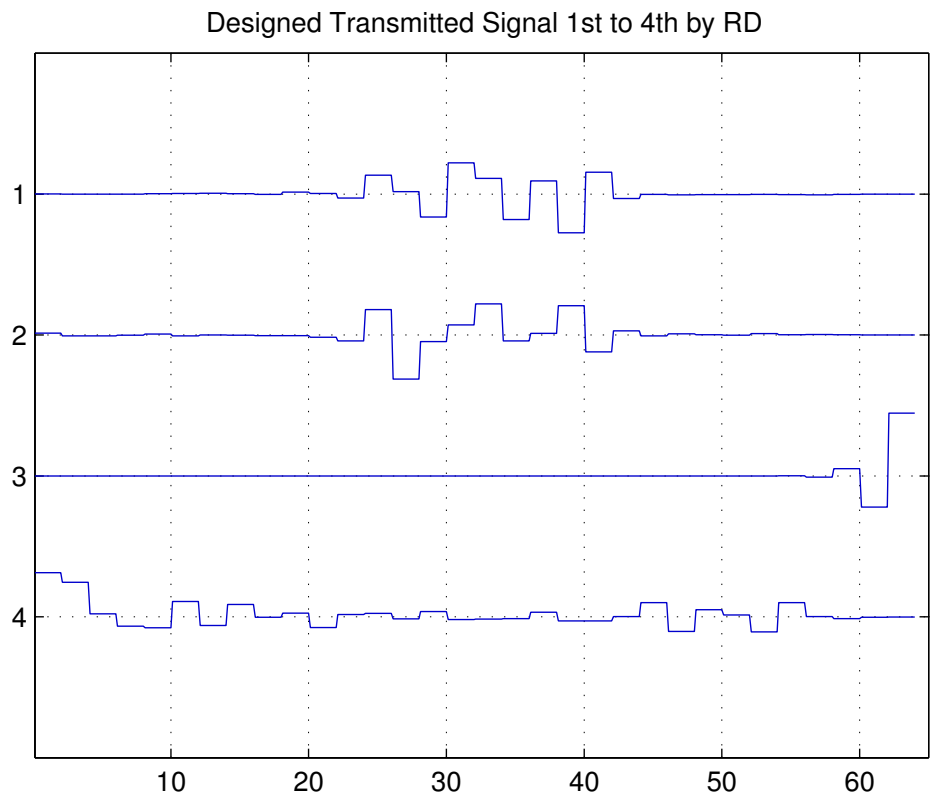

Figure 5.5: Transmitted signals using RD measure, $M = 4$, starting from the Hadamard matrix

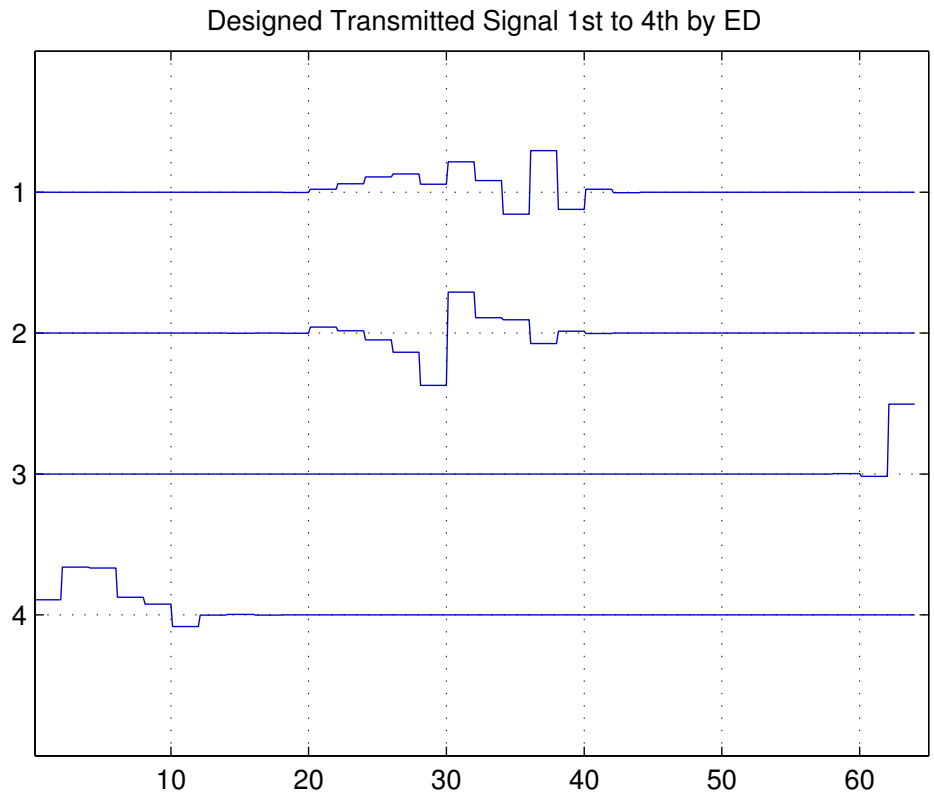

Figure 5.6: Transmitted signals using ED measure, $M = 4$, starting from the Hadamard matrix

Consider the same scenario, but each signal is a linear combination of the cosine functions that are shown in Figure 5.7.

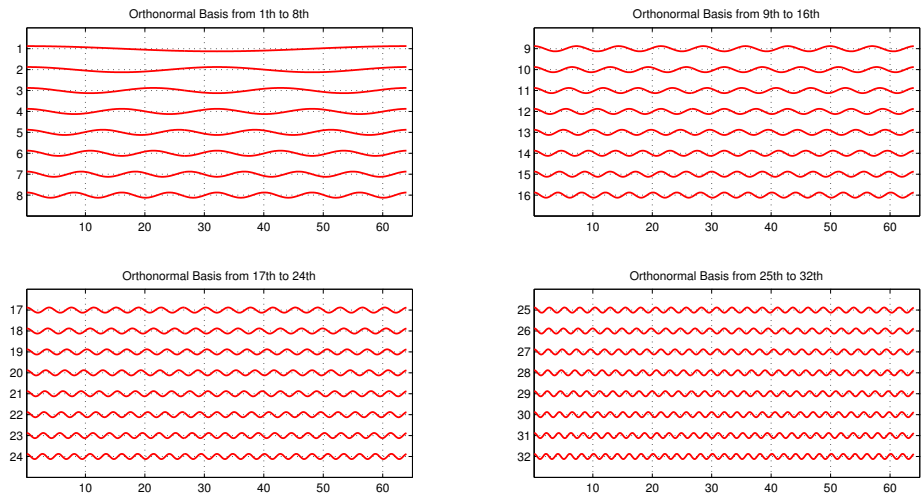

Figure 5.7: First 32 cosine functions

We observe in Figure 5.8 the error between signal covariance and the identity matrices converges to a low level by around 10 iterations for the design measured in RD. On the other hand, using ED to measure the matrix discrepancy takes around 170 iterations to reach a similar level.

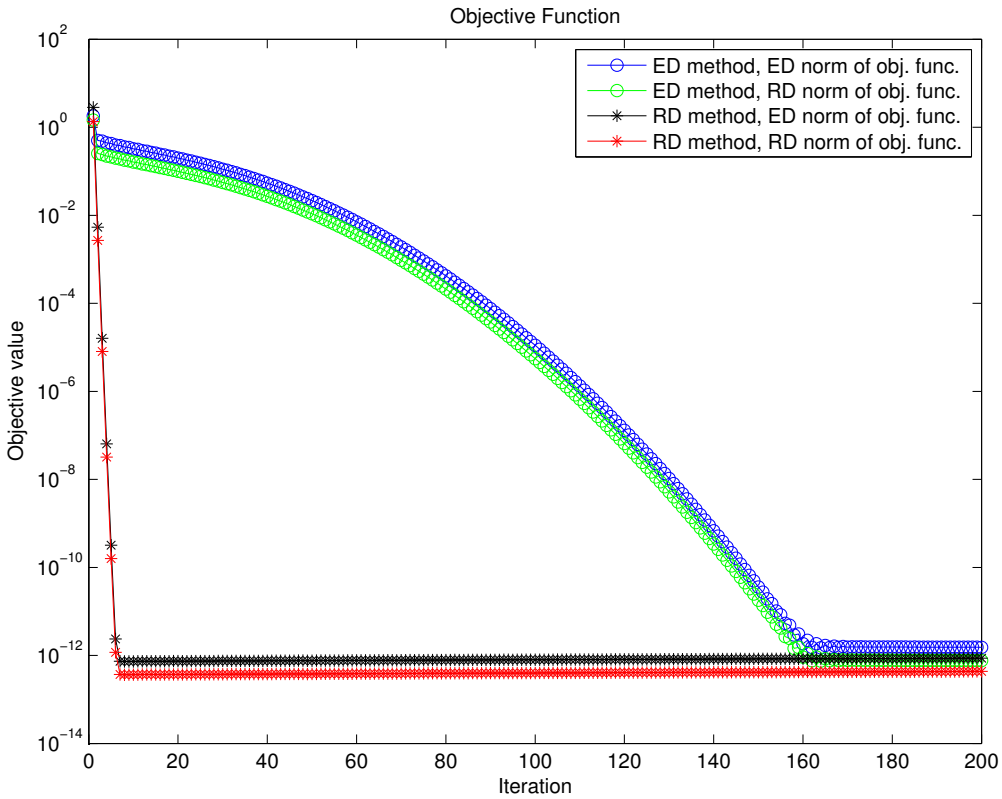

Figure 5.8: Error convergence using cosine functions counting in iterations

Figure 5.9 shows the convergence time (in terms of CPU time) of the design using both ED and RD as measures in the algorithm of Eqs. (2.28). The black and red lines use RD measure (Table 2.1) but compute the estimated error in terms of RD and ED respectively. The blue and green plots use ED measure, but compute the estimated error by RD and ED.

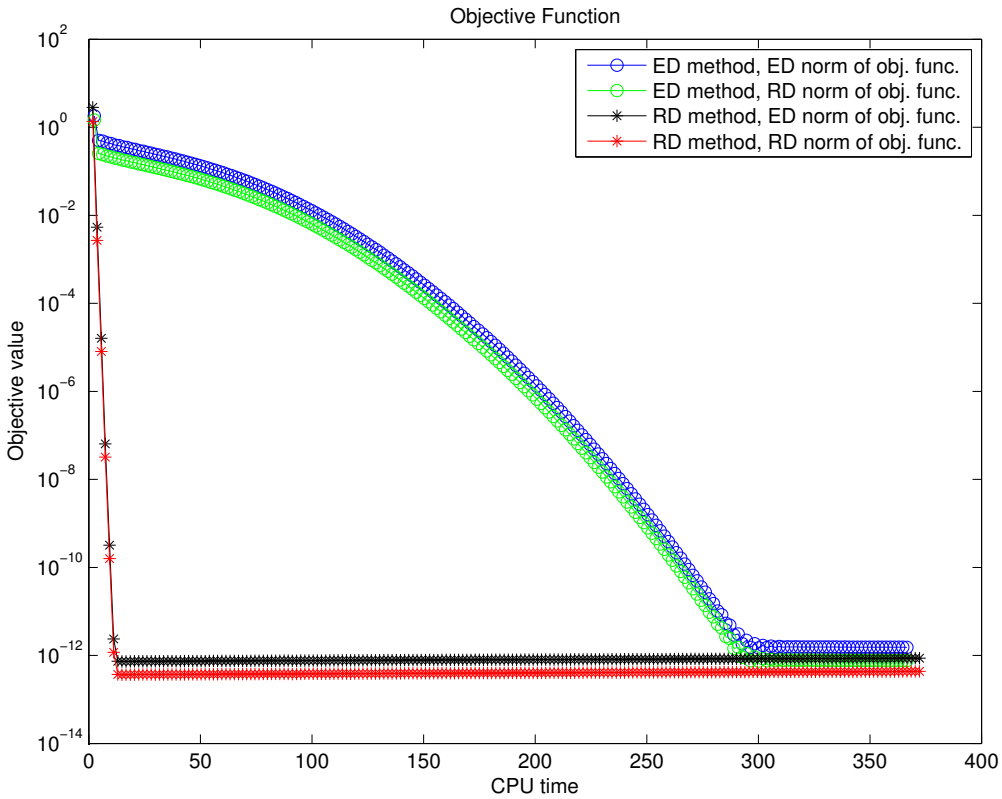

Figure 5.9: Error convergence using cosine functions in length of CPU time

Figure 5.10 illustrates the square norm of correlation with lag τ. The blue plot is the relaxed correlation constraint. The red plot is the square norm of correlation with lag τ using RD measure. The green plot is the square norm of correlation with lag τ using ED measure.

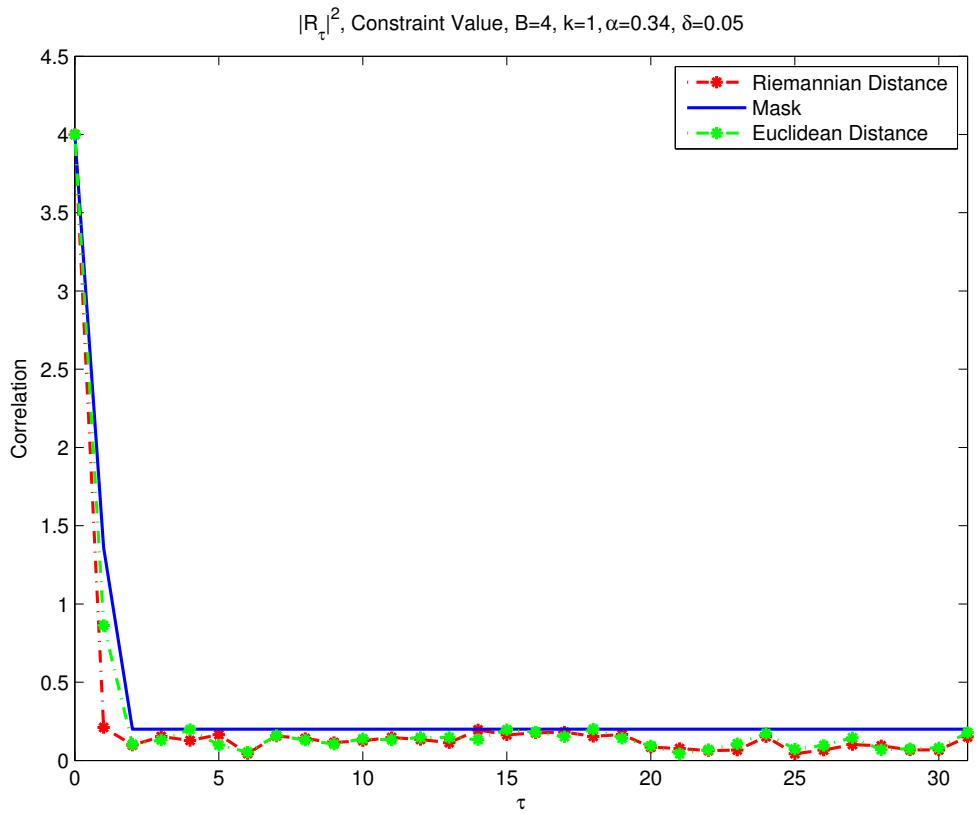

Figure 5.10: Correlation constraints, $\epsilon(1,0) = 0.34M$, $\epsilon(\tau,0) = 0.05M$, $M = 4$

For the case in which we choose a truncated normalized Hadamard matrix as the starting point, the transmitted signals designed using RD measure are shown in Figure 5.11. The transmitted signals designed using the ED measure are shown in Figure 5.12.

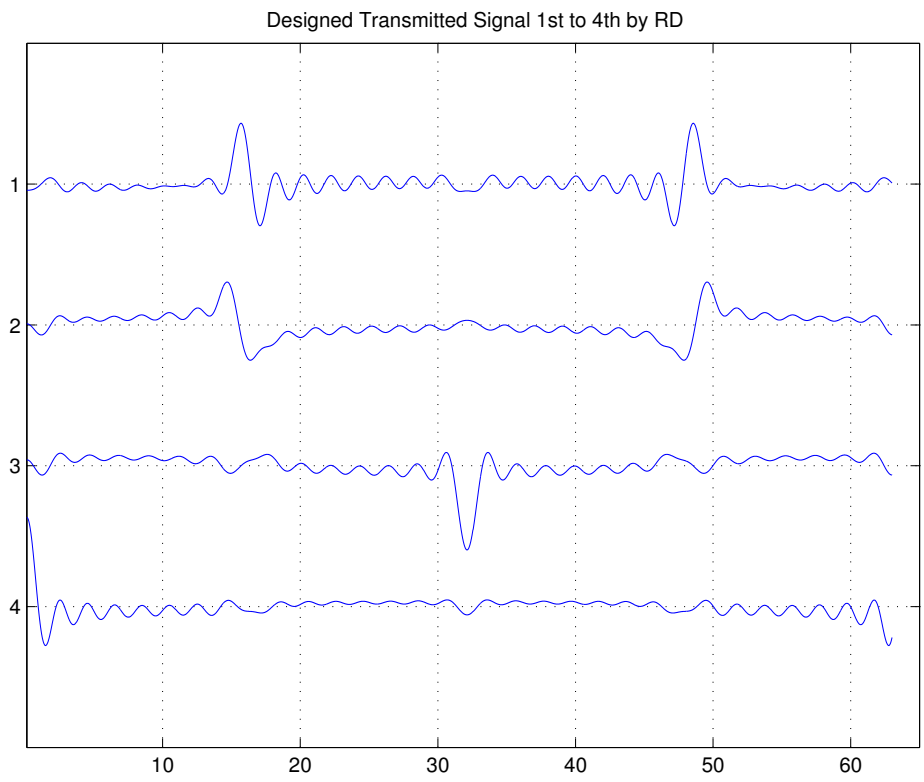

Figure 5.11: Transmitted signals using RD measure, $M = 4$, starting from the Hadamard matrix

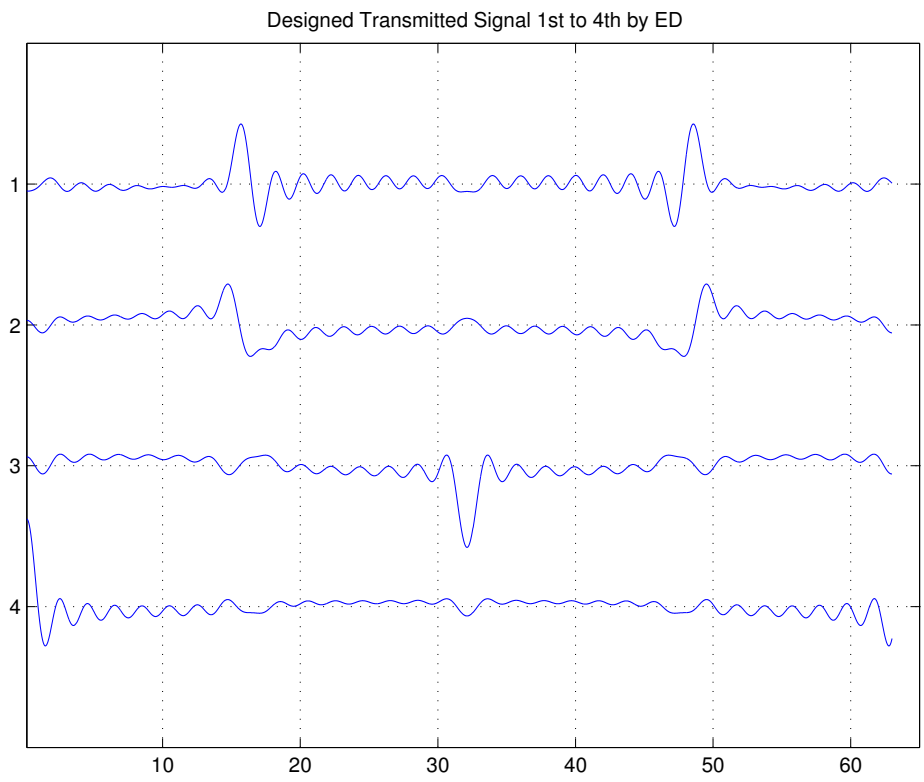

Figure 5.12: Transmitted signals using ED measure, $M = 4$, starting from the Hadamard matrix

The Walsh function has a broad essential bandwidth due to its piecewised structure. The cosine function has relatively broader essential bandwidth compare with the essential bandwidth of WLJ function as WLJ function designed to have the optimal time-bandwidth product. The linear combination of WLJ functions yields signal with narrowest essential bandwidth. Instead of cosine basis, apply WLJ functions. Figure 5.13 illustrates WLJ functions

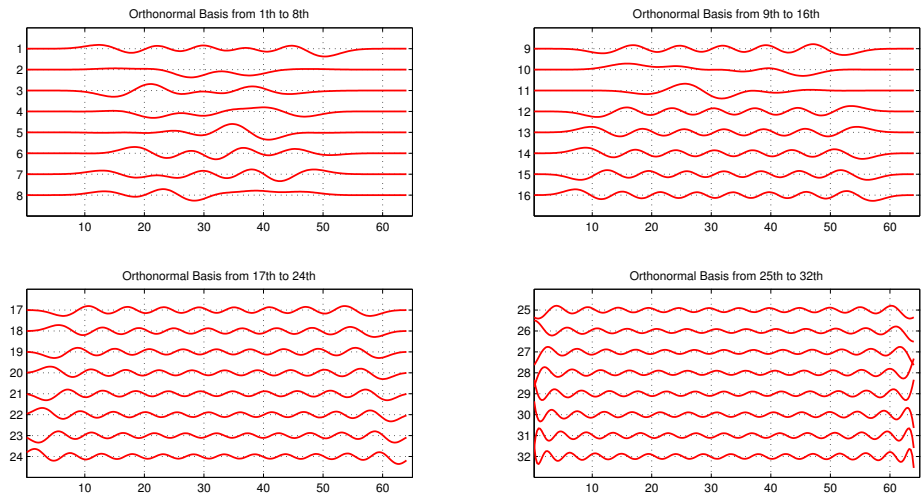

Figure 5.13: First 32 WLJ functions

We observe in Figure 5.14 that the error between signal covariance and the identity matrices converges to a low level by around 20 iterations for the design measured in RD. On the other hand, using ED to measure the matrix discrepancy takes around 140 iterations to reach a similar level. The black and red lines use RD measure (Table 2.1) but compute the estimated error in terms of RD and ED respectively. The blue and green plots use ED measure, but compute the estimated error by RD and ED.

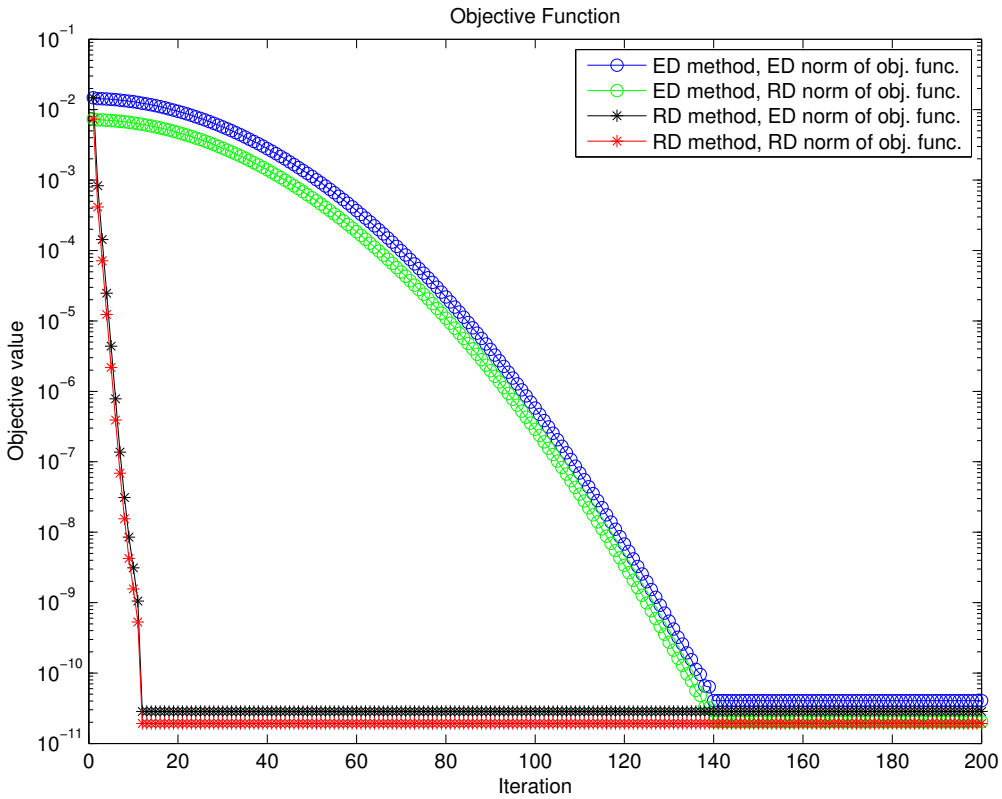

Figure 5.14: Error convergence using WLJ functions counting in iterations

Figure 5.15 shows the convergence time (in terms of CPU time) of the design using both ED and RD as measures in the algorithm of Eqs. (2.28).

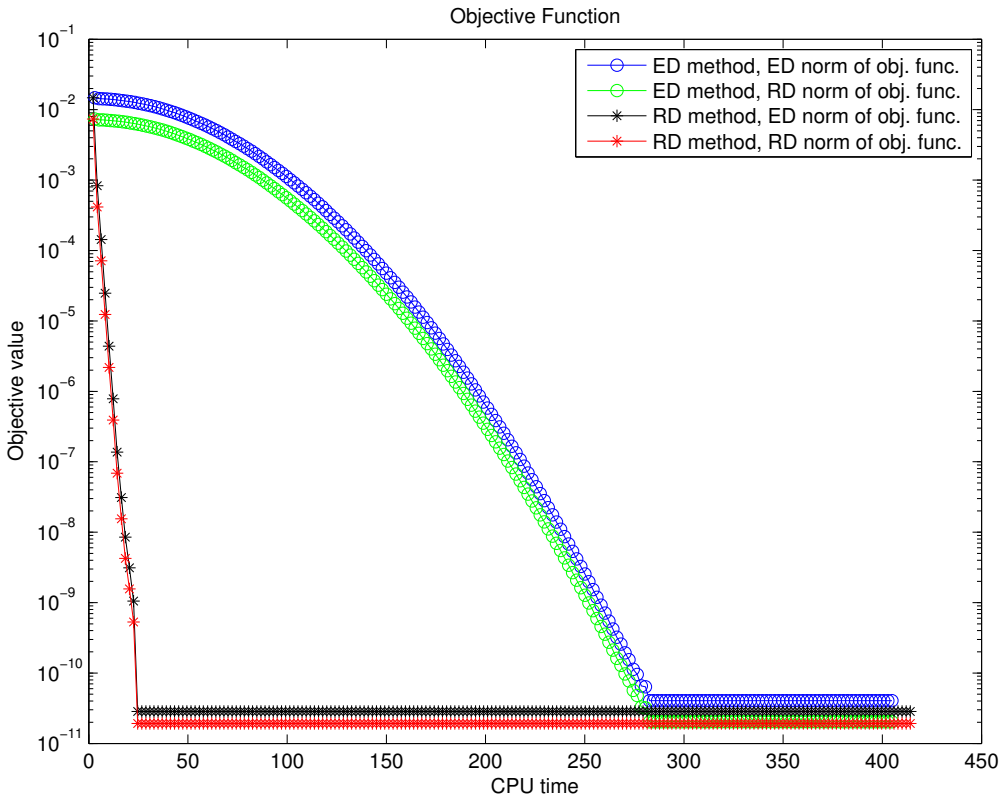

Figure 5.15: Error convergence using WLJ functions in length of CPU time

Figure 5.16 illustrates the square norm of correlation with lag τ. The blue plot is the relaxed correlation constraint. The red plot is the square norm of correlation with lag τ using RD measure. The green plot is the square norm of correlation with lag τ using ED measure.

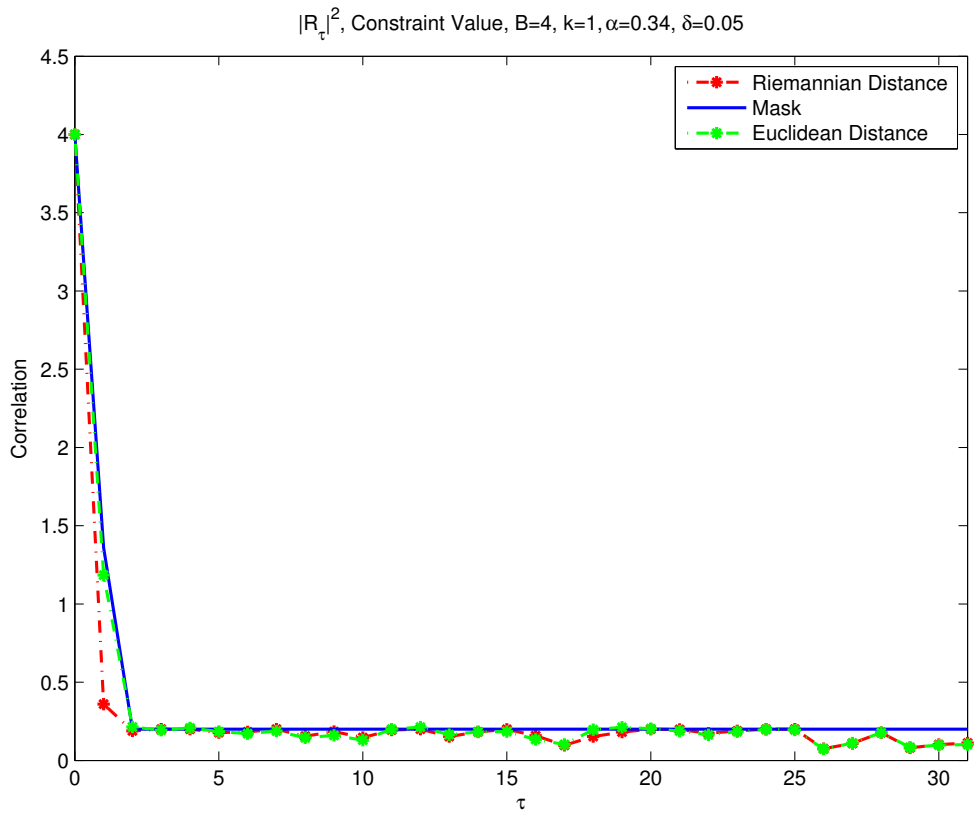

Figure 5.16: Correlation constraints, $\epsilon(1,0) = 0.34M$, $\epsilon(\tau,0) = 0.05M$, $M = 4$

For the case in which we choose a truncated normalized Hadamard matrix as the starting point, the transmitted signals designed using RD measure are shown in Figure 5.17. The transmitted signals designed using ED measure are shown in Figure 5.18.

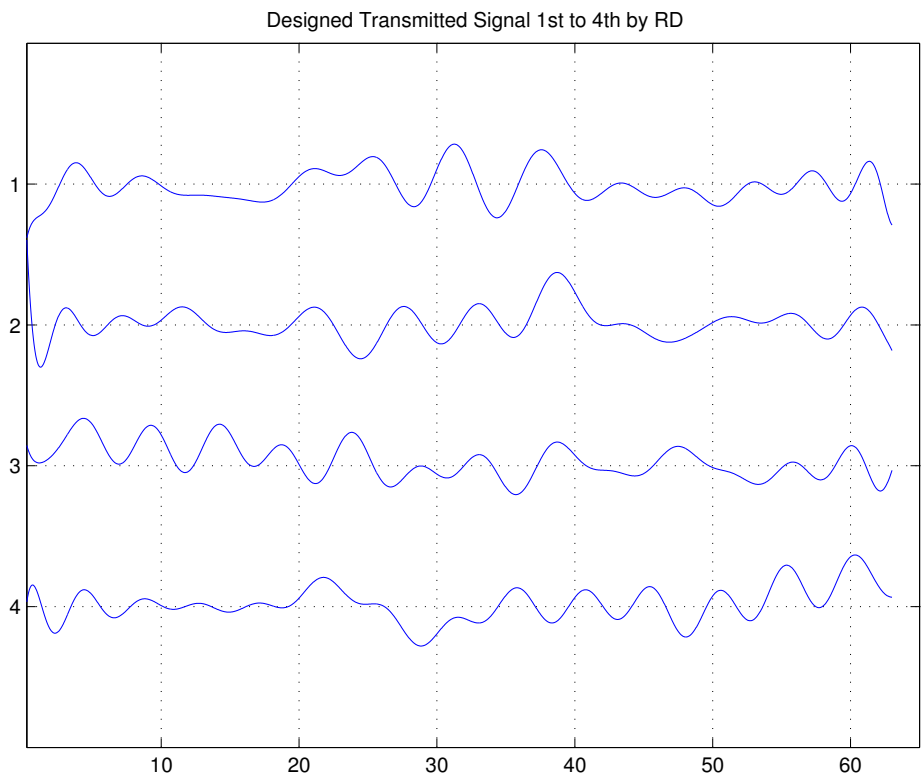

Figure 5.17: Transmitted signals using RD measure, $M = 4$, starting from the Hadamard matrix

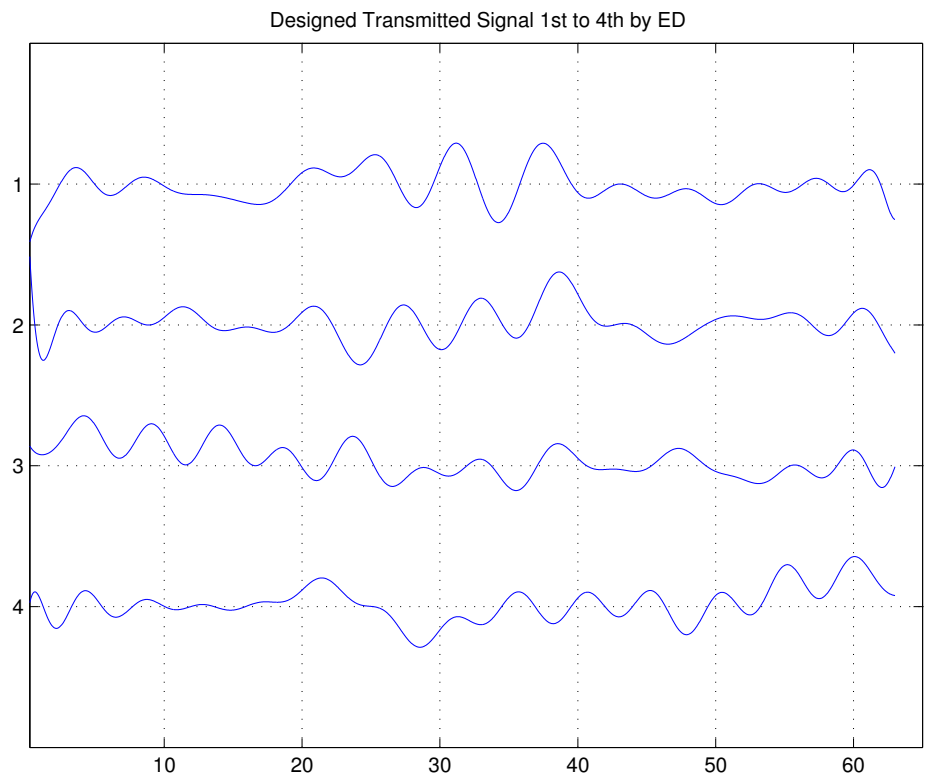

Figure 5.18: Transmitted signals using ED measure, $M = 4$, starting from the Hadamard matrix

5.1.2 Time delay and Doppler frequency shift

Previouly, we set the Doppler frequency shift $\nu = 0$, then the ambiguity matrices become just simply correlation matrices. Here consider both time delay and Doppler frequency shift. Time delay is the delay of returned signal which is related to distance between the target and the antenna array. The Doppler shift is a change in frequency which is related to the velocity of the target. The MIMO radar system has $M = 5$

transmitter antennas for which each transmission waveform is a linear combination of $K = 8$ Walsh functions. Each Walsh function is 16ms in duration. We choose $\epsilon_{\tau,\nu} = 0.4M$ where $\tau \neq 0$ and $\nu \neq 0$. We sample the τ and ν by choosing each sample length as $\tau_s = 0.25\mu s$ and $\nu_s = 0.25 f_c$Hz, $f_c = 5000$Hz. Figure 5.19 the convergence time (in terms of CPU time) of the design using both ED and RD as measures in the algorithm of Eqs. (2.28). The CPU time of each iteration measures the elapsed time of computation and expression transformation by CVX [22] in each iteration in unit of second. An Explanation of the faster convergence of using the RD measure has been given in Section 2.5. The black and red lines use RD measure (Table 2.1) but compute the estimated error in terms of RD and ED respectively. The blue and green plots use ED measure, but compute the estimated error by RD and ED. An explanation of the faster convergence of using the RD measure has been given in Section 2.5.

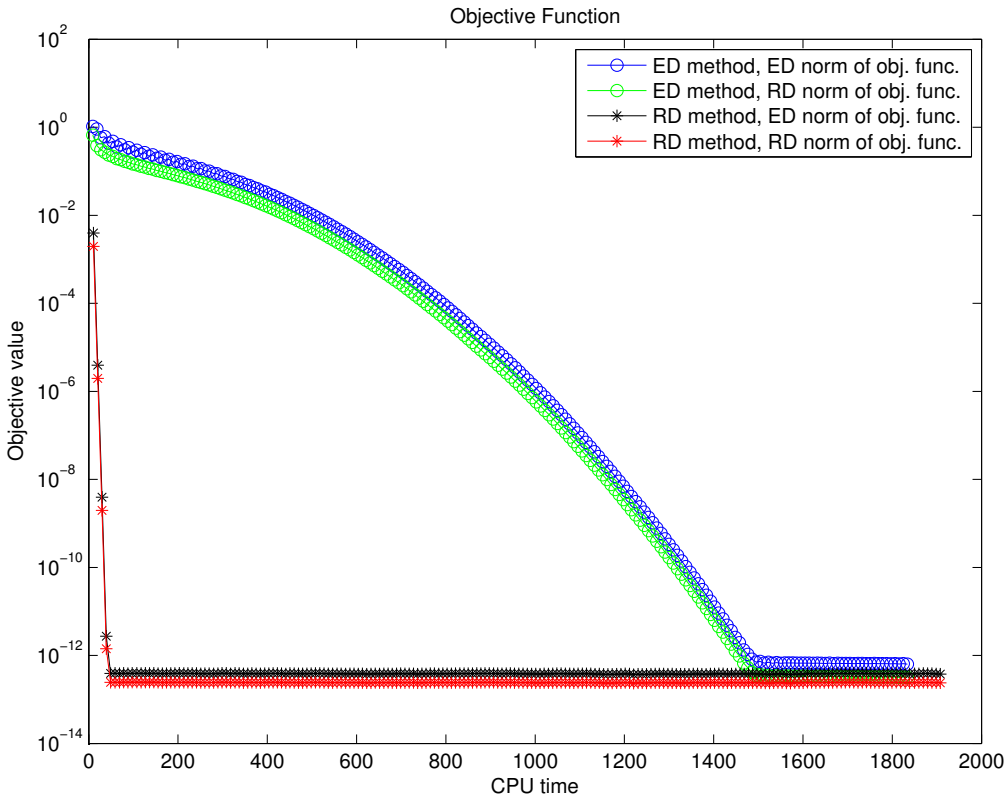

Figure 5.19: Error convergence using Walsh functions in length of CPU time

The function of the square norm of the ambiguity matrix is a two dimentional function with τ and ν. Figure 5.20 illustrates vectorized version of the square norm of the ambiguity matrix with lag τ and ν. The blue plot is the relaxed correlation constraint. The red plot is the square norm of ambiguity matrix with lag τ and ν using RD measure. The black plot is the square norm of ambiguity matrix with lag τ and ν using ED measure.

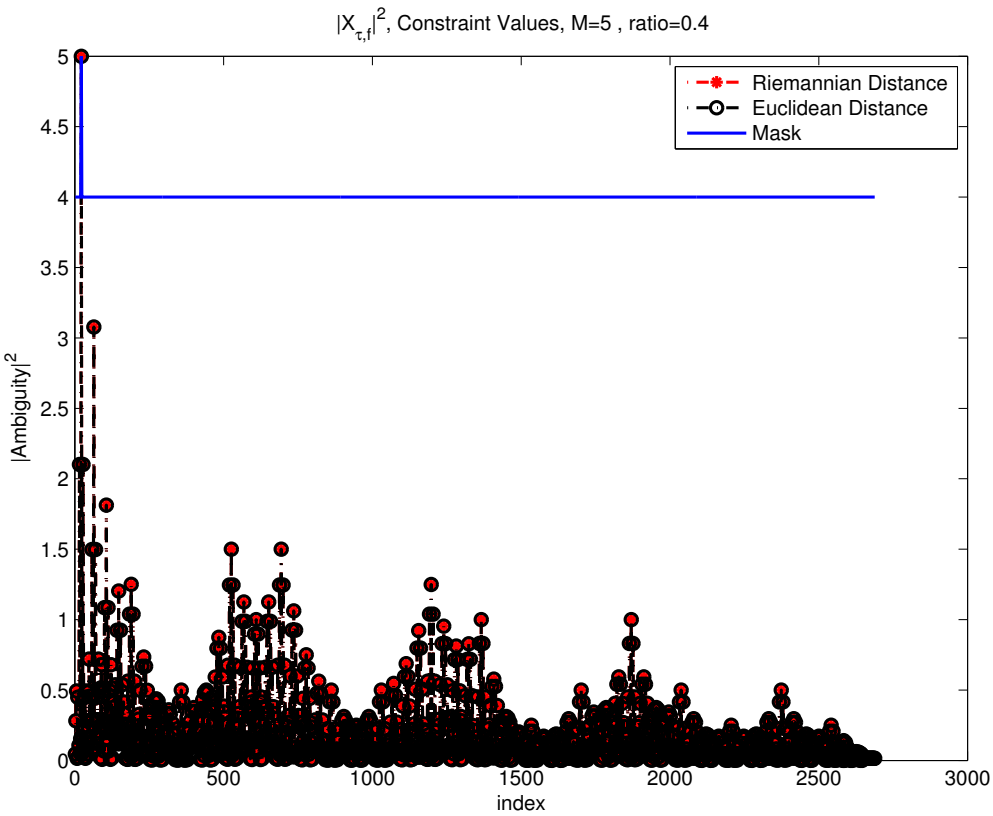

Figure 5.20: Sidelobe constraints, $\epsilon(\tau \neq 0, \nu \neq 0) = 0.4M$, $M = 5$

For the case in which we choose a truncated normalized Hadamard matrix as the starting point, the transmitted signals designed using RD measure are shown in Figure 5.21. The transmitted signals designed using ED measure are shown in Figure 5.22.

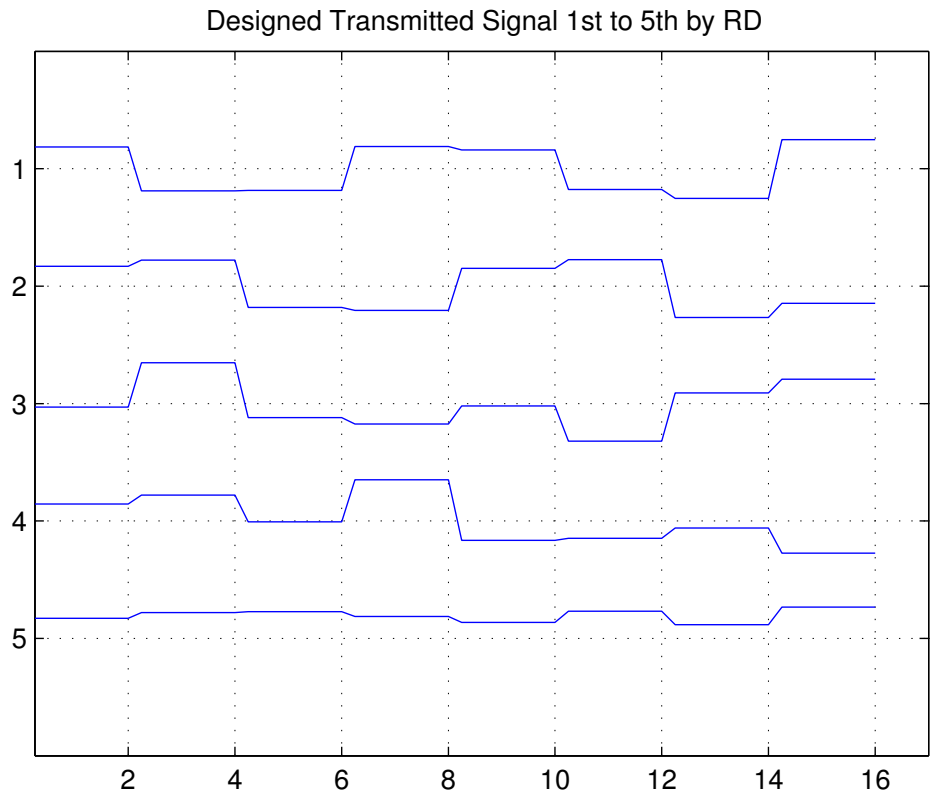

Figure 5.21: Transmitted signals using RD measure, $M = 5$, starting from the Hadamard matrix

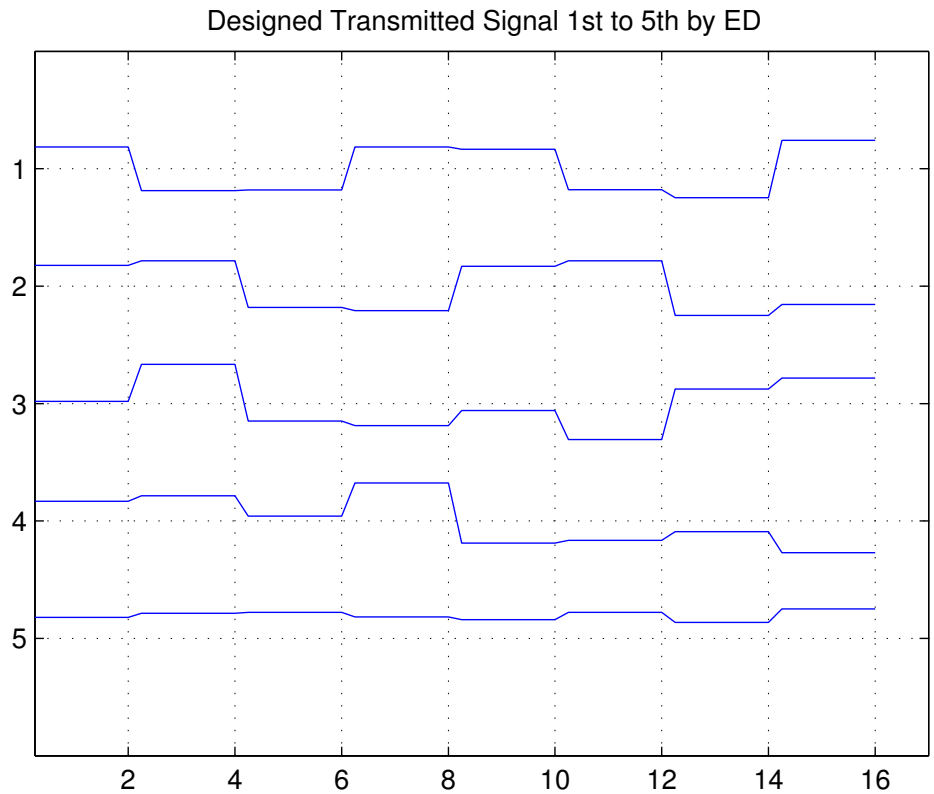

Figure 5.22: Transmitted signals using ED measure, $M = 5$, starting from the Hadamard matrix

Next, we apply the cosine set to the synthesize transmitted waveforms. Each waveform is a linear combination of cosine functions. Figure 5.23 the convergence time (in terms of CPU time) of the design using both ED and RD as measures in the algorithm of Eqs. (2.28). The black and red lines use RD measure (Table 2.1) but compute the estimated error in terms of RD and ED respectively. The blue and green plots use ED measure, but compute the estimated error by RD and ED.

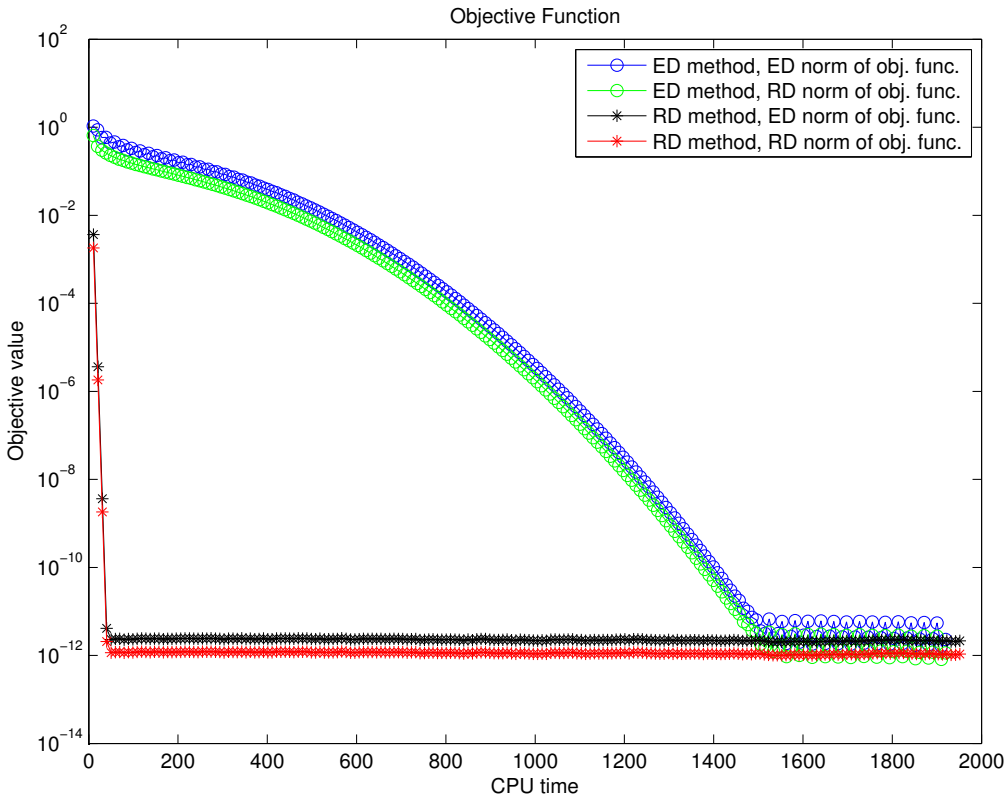

Figure 5.23: Error convergence using cosine functions in length of CPU time

Figure 5.24 illustrates the square norm of ambiguity matrix with lag τ and ν. The red plot is the square norm of ambiguity matrix with lag τ and ν using RD measure. The black plot is the square norm of ambiguity matrix with lag τ and ν using ED measure.

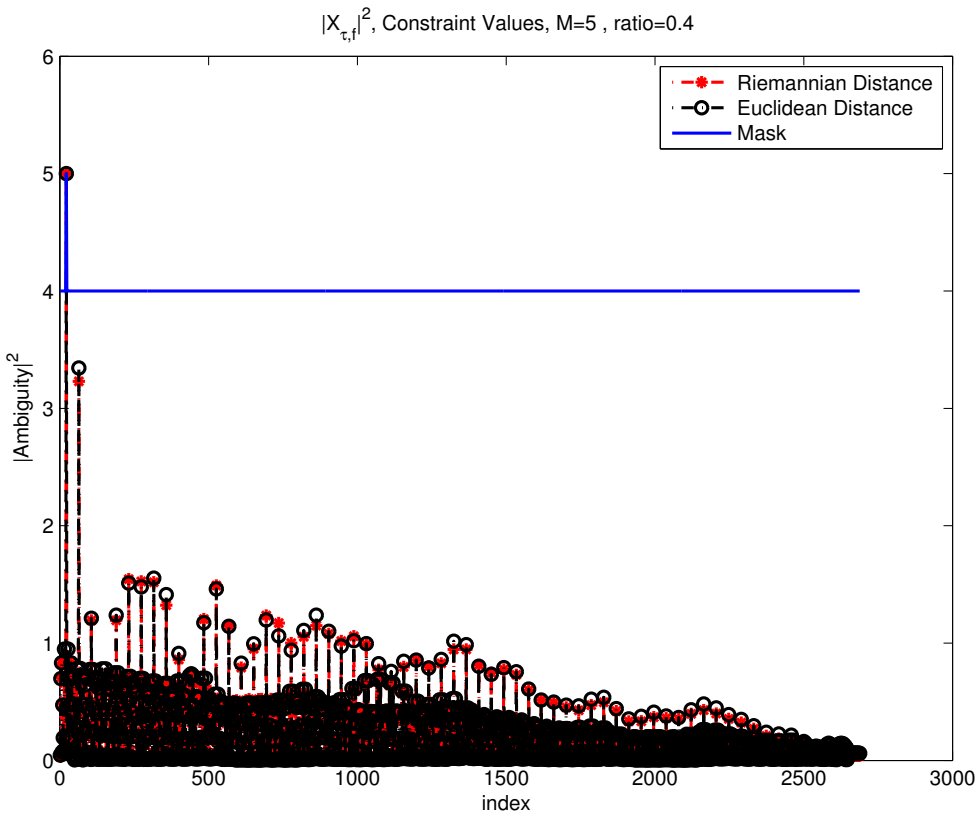

Figure 5.24: Sidelobe constraints, $\epsilon(\tau \neq 0, \nu \neq 0) = 0.4M$, $M = 5$

For the case in which we choose a truncated normalized Hadamard matrix as the starting point, the transmitted signals designed using RD measure are shown in Figure 5.25. The transmitted signals designed using ED measure are shown in Figure 5.26.

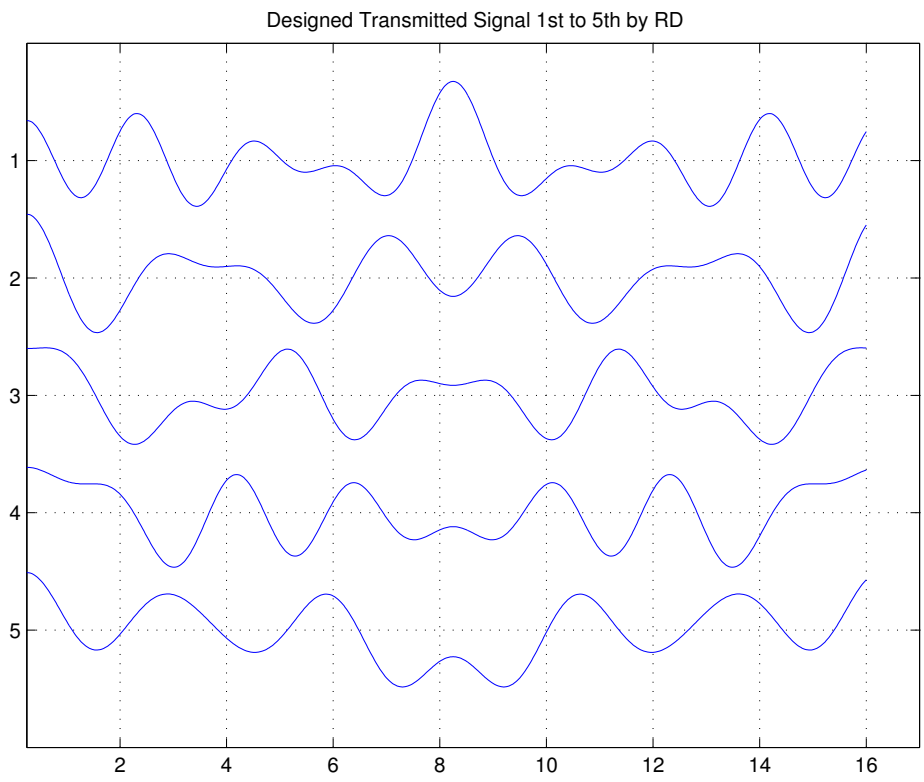

Figure 5.25: Transmitted signals using RD measure, $M = 5$, starting from the Hadamard matrix

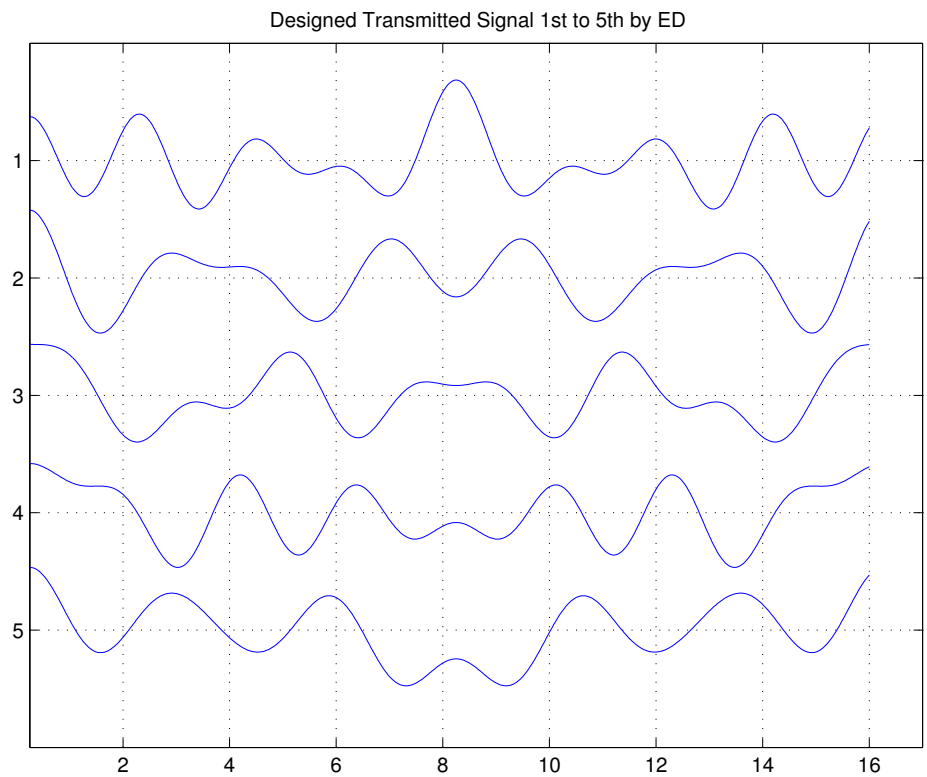

Figure 5.26: Transmitted signals using RD measure, $M = 5$, starting from the Hadamard matrix

For the same scenario, instead of Walsh or cosine sets, we now apply the WLJ set to the design. Each waveform is a linear combination of WLJ functions. Figure 5.27 illustrates the convergence time (in terms of CPU time) of the design using both ED and RD as measures in the algorithm of Eqs. (2.28). The black and red lines use RD measure (Table 2.1) but compute the estimated error in terms of RD and ED respectively. The blue and green plots use ED measure, but compute the estimated error by RD and ED.

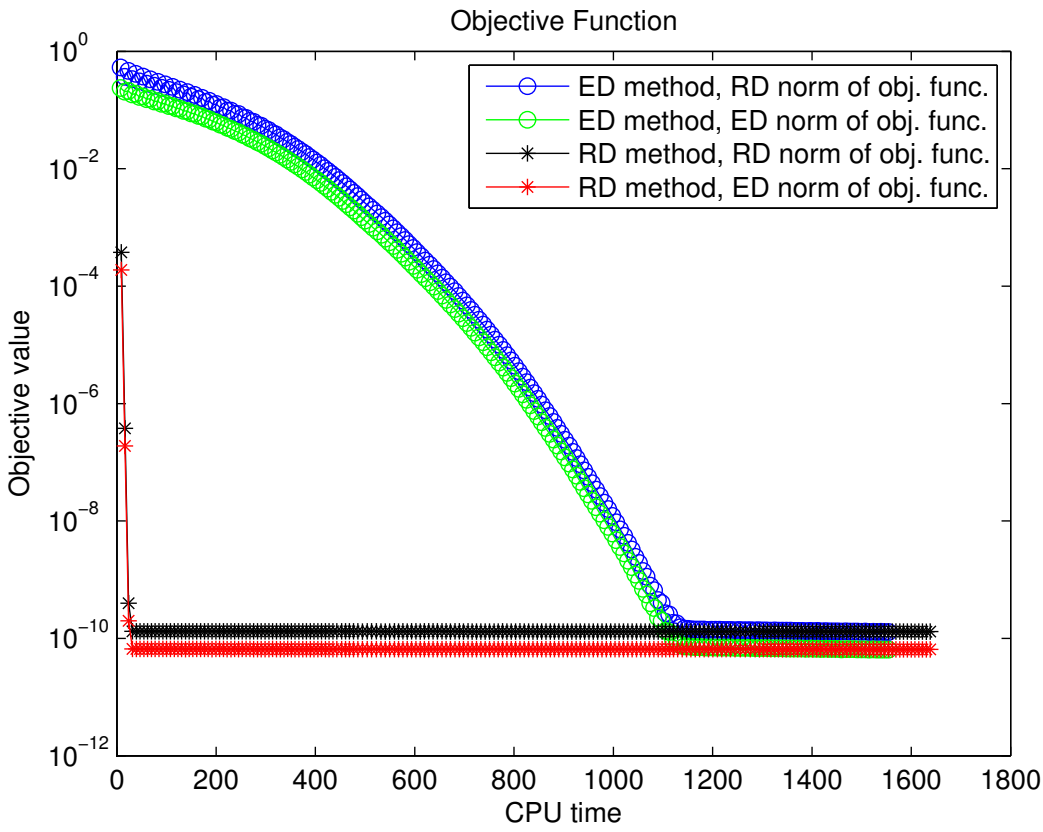

Figure 5.27: Error convergence using WLJ functions in length of CPU time

Figure 5.28 illustrates the square norm of ambiguity matrix with lag τ and ν. The red plot is the square norm of ambiguity matrix with lag τ and ν using RD measure. The black plot is the square norm of ambiguity matrix with lag τ and ν using ED measure.

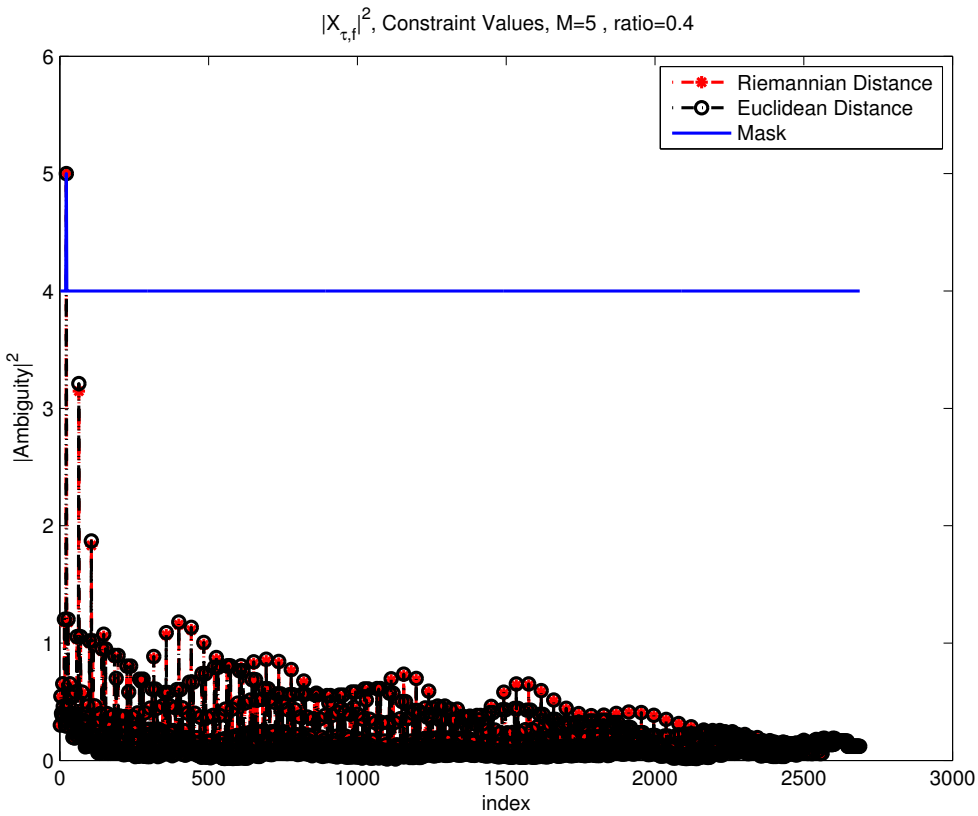

Figure 5.28: Sidelobe constraints, $\epsilon(\tau \neq 0, \nu \neq 0) = 0.4M$, $M = 5$

For the case in which we choose a truncated normalized Hadamard matrix as the starting point, the transmitted signals designed using RD measure are shown in Figure 5.29. The transmitted signals designed using ED measure are shown in Figure 5.30.

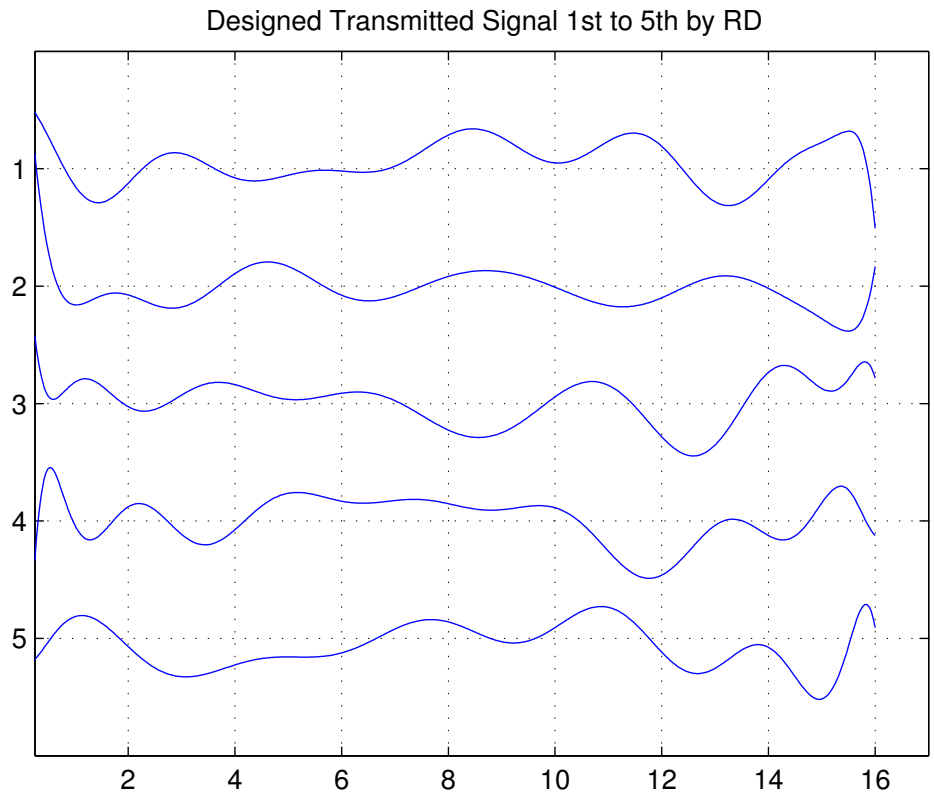

Figure 5.29: Transmitted signals using RD measure, $M = 5$, starting from the Hadamard matrix

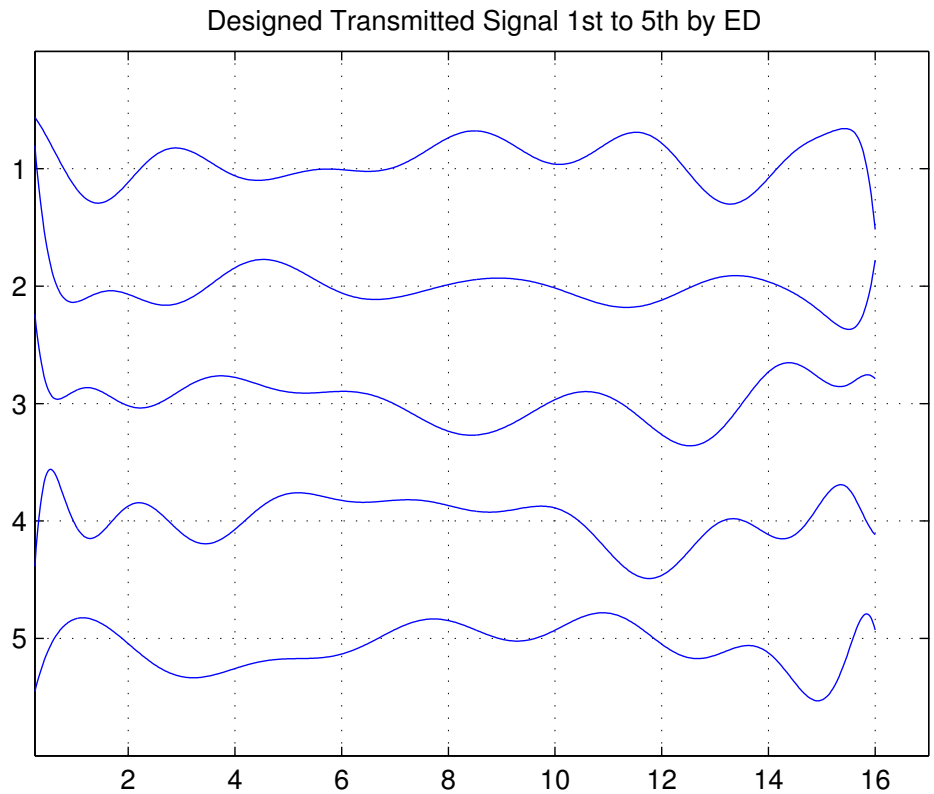

Figure 5.30: Transmitted signals using ED measure, $M = 5$, starting from the Hadamard matrix

The difference between the two transmission signals using RD and ED is very small due to the rather loose constraint that $\epsilon(\tau, \nu) = 0.4M$. If this constraint be made tighter, the difference between the two signals designed with different distance measures may be more conspicuous.

5.2 Detection and Estimation Results using Walsh Functions, Cosine Functions and WLJ Functions

5.2.1 Simulation Environment

Fix N targets at different locations with different velocities coming from 30° in direction. To test on designed signals, we do an experiment of detection and parameter estimation on fixed targets using designed signals. If we have three targets coming from 30° direction. Figure. 5.31 shows an example of locations of targets.

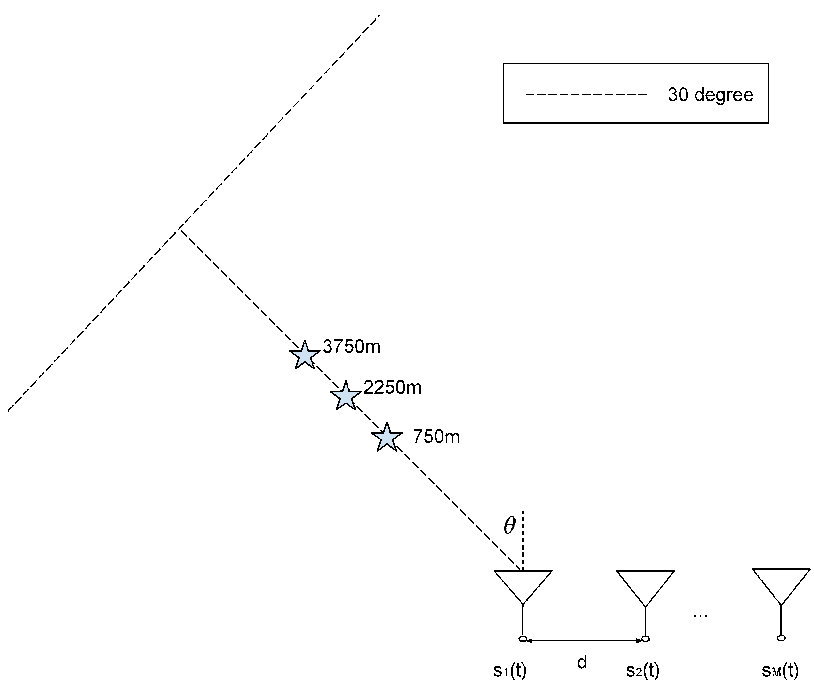

Figure 5.31: An example of locations of targets

The transmitting steering vector is

$$\boldsymbol{a} = \begin{bmatrix} 1 & e^{j2\pi\sin(\theta)} & \dots & e^{j2\pi(M-1)\sin(\theta)} \end{bmatrix}^T, \tag{5.2}$$

where θ is the angle of arriving direction of targets. The receiving steering vector is

$$\boldsymbol{b} = \begin{bmatrix} 1 & e^{j2\pi\sin(\theta_s)} & \dots & e^{j2\pi(M-1)\sin(\theta_s)} \end{bmatrix}^T, \tag{5.3}$$

where θ_s is the estimated angle of arriving direction of targets. In this thesis, we focus on the estimation of target distance and velocity, we set $\theta = \theta_s$ as known.

At receiver array, we calculate the ambiguity,

$$F_R(\tau_s, \nu_s) = \boldsymbol{a}\boldsymbol{X}_R\boldsymbol{X}_T^H(\tau_s, \nu_s)\boldsymbol{b}^H, \tag{5.4}$$

where $\boldsymbol{X}_R$ is a vector of the received signals, $\boldsymbol{X}_T^H(\tau_s, \nu_s)$ is a vector of shifted version of the transmitted signals, τ_s is the shifted time, and ν_s is the shifted Doppler frequency [12].

5.2.2 Time delay only

Any local maximum of correlation $F_R(\tau, 0)$ between received signals and time-shifted transmission signal is greater than a threshold, it is considered as a target candidate. Any target candidate that is recognized over 50% in time, it is confirmed as a detected target. The threshold is determined by Neyman-Pearson criterion fixing the false alarm percentage at a certain rate. Then the probability of false alarm error is fixed. In this experiment we test on 10 scans and if the target candidate is recognized

over 5 times, we confirm it as a detected target. The tolerance percentage 50% is chosen by experiment. The N simulated targets are point targets which are located at distances $d_1, d_2, \ldots, d_N$ from the reference point of the radar antenna array. For each set of transmitted signal estimating the distance of the N targets, we define an mean square relative error of distance estimation as

$$\bar{e}_d^2 = \frac{1}{N}\left[\left(\frac{e_{d_1}}{d_1}\right)^2 + \ldots \left(\frac{e_{d_N}}{d_N}\right)^2\right] \tag{5.5}$$

Tables 5.1, 5.2, 5.3 show the mean square relative errors of distance in estimation using ED and RD algorithms using Walsh, cosine and WLJ functions. Note, the "M" means target missed in the detection.

Table 5.1: $\bar{e}_d^2$ using Walsh functions

Shortest distance between 2 adj. targets	1500m	750m	157.5m	150m
Optimum RD (200 iterations)	9.34E-05%	1.48E-04%	3.88E-04%	2.83E-04%
Optimum RD (10 iterations)	9.34E-05%	1.48E-04%	3.88E-04%	2.60E-04%
Optimum ED (200 iterations)	9.34E-05%	1.48E-04%	4.81E-04%	4.87E-04%
Non-optimum ED (10 iterations)	9.34E-05%	1.48E-04%	M	M

Table 5.2: $\bar{e}_d^2$ using cosine functions

Shortest distance between 2 adj. targets	1500m	750m	157.5m	150m
Optimum RD (200 iterations)	9.34E-05%	1.48E-04%	1.72E-04%	2.83E-04%
Optimum RD (10 iterations)	9.34E-05%	1.48E-04%	1.72E-04%	2.60E-04%
Optimum ED (200 iterations)	9.34E-05%	1.48E-04%	2.66E-04%	4.66E-04%
Non-optimum ED (10 iterations)	9.34E-05%	1.48E-04%	M	M

Table 5.3: $\bar{e}_d^2$ using WLJ functions

Shortest distance between 2 adj. targets	1500m	750m	157.5m	150m
Optimum RD (200 iterations)	9.34E-05%	1.48E-04%	1.72E-04%	2.60E-04%
Optimum RD (10 iterations)	9.34E-05%	1.48E-04%	1.72E-04%	2.60E-04%
Optimum ED (200 iterations)	9.34E-05%	1.48E-04%	2.66E-04%	2.83E-04%
Non-optimum ED (10 iterations)	9.34E-05%	1.48E-04%	M	M

Detection results

As we have explained the reason for the fast convergence of the iterative technique that uses the RD measure in Section 2.5. After 10 iterations, the error between estimated covariance matrix and identity using RD measure has converged and the correlation between any arbitrary pair of antennas is close to zero. However, after 10 iterations of the technique that uses the ED measure, the technique has not converged and the error is about 10^8 larger than the error using RD measure. Hence, there is a relatively large interference between any two antennas using ED measure. For all the three orthonormal function sets, when any adjacent targets are close, the system transmitting waveforms using ED measure may have missing target detection.

Estimation results

It can be observed that for all the three orthonormal function sets, the use of RD as the design measure of the covariance matrix offers higher accuracies in the estimation of target distance than the use of ED especially in the cases when the targets are close together. It can also be observed that in the cases of close targets, the optimum signal synthesized using the WLJ functions yields the most accurate estimates.

5.2.3 Time delay and Doppler frequency shift

The joint estimation of target distance and target velocity utilizes the local maxima on the ambiguity function with τ and ν. For velocity estimation we define the mean square relative error similar to that of the distance estimation in (5.5) such that

$$\bar{e}_v^2 = \frac{1}{N}\left[\left(\frac{e_{v_1}}{v_1}\right)^2 + \ldots \left(\frac{e_{v_N}}{v_N}\right)^2\right] \tag{5.6}$$

where v_n is the velocity of target n with reference to the antenna array and e_{v_n} is the velocity estimation error with respect to target n, $n = 1, 2, \ldots, N$, with N being the number of detected targets. Tables 5.4, 5.5 and 5.6 show the mean square relative errors in distance and velocity estimation using ED and RD measures synthesized by Walsh, cosine and WLJ functions. Note, that the "M" means missing target in detection.

Table 5.4: $\bar{e}_d^2 + \bar{e}_v^2$ using Walsh functions

Distances and Velocities of targets	(750m, 420m/s) (1050m, 480m/s) (1350m, 540m/s)	(1500m, 480m/s) (1515m, 510m/s) (1530m, 540m/s)	(1500m, 510m/s) (1515m,525m/s) (1530m,540m/s)	(1500m, 525m/s) (1515m,532.5m/s) (1530m,540m/s) (1545m,543.6m/s)
Optimum RD (200 iterations)	0%	3.26E-04%	2.03E-03%	4.17E-03%
Optimum RD (10 iterations)	0%	3.26E-04%	2.03E-03%	4.17E-03%
Optimum ED (200 iterations)	0%	3.26E-04%	2.03E-03%	6.02E-03%
Non-optimum ED (10 iterations)	0%	3.15E-03%	5.71E-03%	M

Table 5.5: $\bar{e}_d^2 + \bar{e}_v^2$ using cosine functions

Distances and Velocities of targets	(750m, 420m/s) (1050m, 480m/s) (1350m, 540m/s)	(1500m, 480m/s) (1515m, 510m/s) (1530m, 540m/s)	(1500m, 510m/s) (1515m,525m/s) (1530m,540m/s)	(1500m, 525m/s) (1515m,532.5m/s) (1530m,540m/s) (1545m,543.6m/s)
Optimum RD (200 iterations)	0%	3.26E-04%	2.03E-03%	3.49E-03%
Optimum RD (10 iterations)	0%	3.26E-04%	2.03E-03%	3.49E-03%
Optimum ED (200 iterations)	0%	3.26E-04%	2.03E-03%	5.67E-03%
Non-optimum ED (10 iterations)	0%	3.14E-03%	5.71E-03%	M

Table 5.6: $\bar{e}_d^2 + \bar{e}_v^2$ using WLJ functions

Distances and Velocities of targets	(750m, 420m/s) (1050m, 480m/s) (1350m, 540m/s)	(1500m, 480m/s) (1515m, 510m/s) (1530m, 540m/s)	(1500m, 510m/s) (1515m,525m/s) (1530m,540m/s)	(1500m, 525m/s) (1515m,532.5m/s) (1530m,540m/s) (1545m,543.6m/s)
Optimum RD (200 iterations)	0%	3.26E-04%	2.03E-03%	3.23E-03%
Optimum RD (10 iterations)	0%	3.26E-04%	2.03E-03%	3.23E-03%
Optimum ED (200 iterations)	0%	3.26E-04%	2.03E-03%	5.09E-03%
Non-optimum ED (10 iterations)	0%	3.14E-03%	5.71E-03%	M

The joint estimation performance of the transmission signals synthesized with the three types of orthonormal functions are similar to those for the estimation of distance alone. That is, the use of ED as design measure with incomplete convergence will have missing target detection and the use of RD as the design measure of the covariance matrix offers higher accuracies in the joint estimation than the use of ED especially when the targets are close. Also, in the cases of close adjacent targets, the optimum signal synthesized using WLJ functions yields the most accurate estimates.

If we do the optimization off-line, then the fast rate of convergence may not be

a great advantage for the technique using RD measure. However if we make the sidelobe constraint tighter, for example, $\epsilon(1,0) = 0.34M$, $\epsilon(\tau,0) = 0.02M$, Figure 5.32 illustrates the convergence time (in terms of CPU time) of the design using both ED and RD as measures in the algorithm of Eqs. (2.28). The black and red lines use RD measure (Table 2.1) but compute the estimated error in terms of RD and ED respectively. The blue and green plots use ED measure, but compute the estimated error by RD and ED.

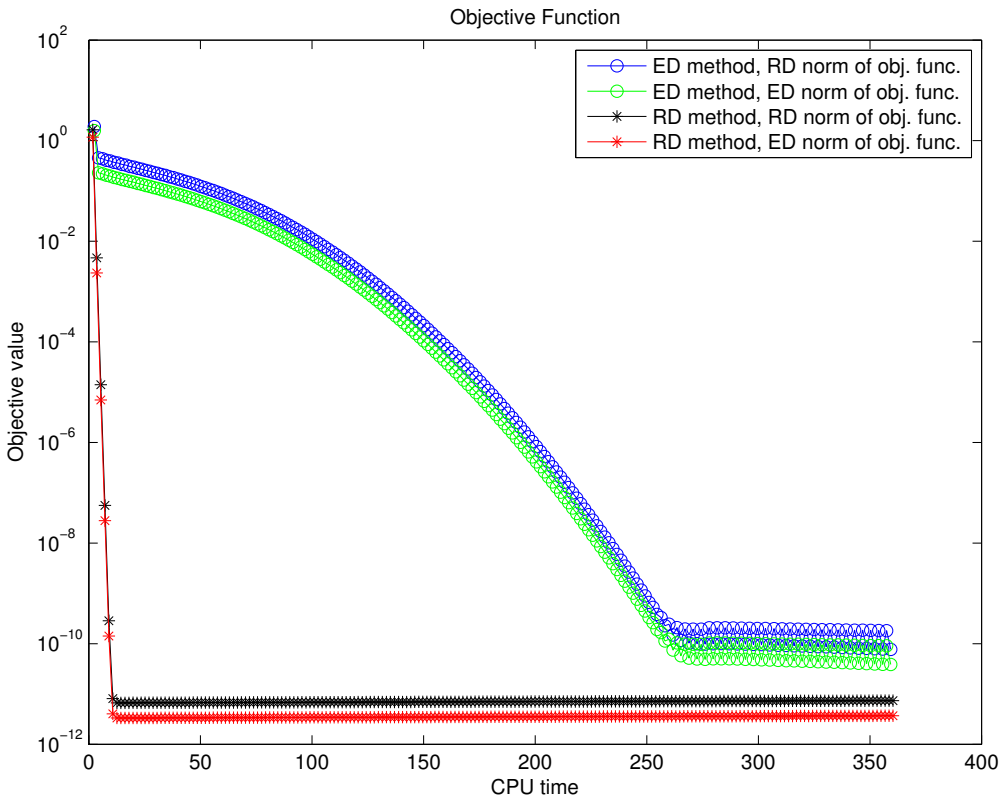

Figure 5.32: Error convergence using Walsh functions in length of CPU time

We observe that the technique using ED has a larger converged error compare to

the technique using RD measure. It means the designed signals using ED measure have larger interference between any arbitrary pair of antennas. The estimation will be less accurate if the interferrence increases. Table 5.7 shows the mean square relative errors of distance in estimation using ED and RD algorithms using Walsh with a tighter constraint.

Table 5.7: $\bar{e}_d^2$ using Walsh functions

Shortest distance between 2 adj. targets	1500m	750m	157.5m	150m
Optimum RD (200 iterations)	9.34E-05%	1.48E-04%	1.72E-04%	2.60E-04%
Optimum RD (10 iterations)	9.34E-05%	1.48E-04%	1.72E-04%	2.60E-04%
Optimum ED (200 iterations)	9.34E-05%	1.48E-04%	4.82E-04%	8.71E-04%
Non-optimum ED (10 iterations)	9.34E-05%	1.48E-04%	M	M

5.3 Bandwidth Optimization with the three function sets

As we mentioned in Chapter 3, the bandwidth constraint is nessesary in practical situations. We require to design signals which is finite in both time duration and in essential bandwidth.

5.3.1 Power spectrum density of tranmitted signal using different orthonormal sets

For example, using optimization (3.3), if we fix $\alpha = 0.1$, $\epsilon(1,0) = \alpha M$ and $\epsilon(\tau,0) = (\alpha/2)M$, and set the bandwidth at 1860Hz, 484Hz and 234Hz while applying Walsh, cosine and WLJ sets respectively, then the errors will converge to around 10^{-9} using

Walsh, cosine and WLJ sets. Figure 5.33 shows the power spectrum densities of four transmitted signals with Walsh functions when $f_0 = 1860Hz$

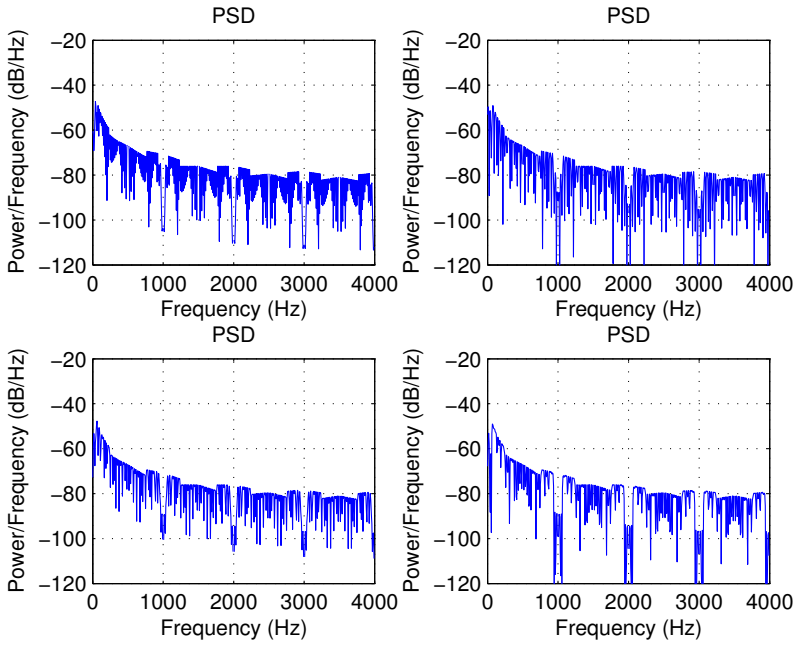

Figure 5.33: The PSD of four transmitted signals constructed from Walsh functions, f_0=1860Hz

Figure 5.34 shows the power spectrum densities of four transmitted signals with cosine functions when $f_0 = 484Hz$

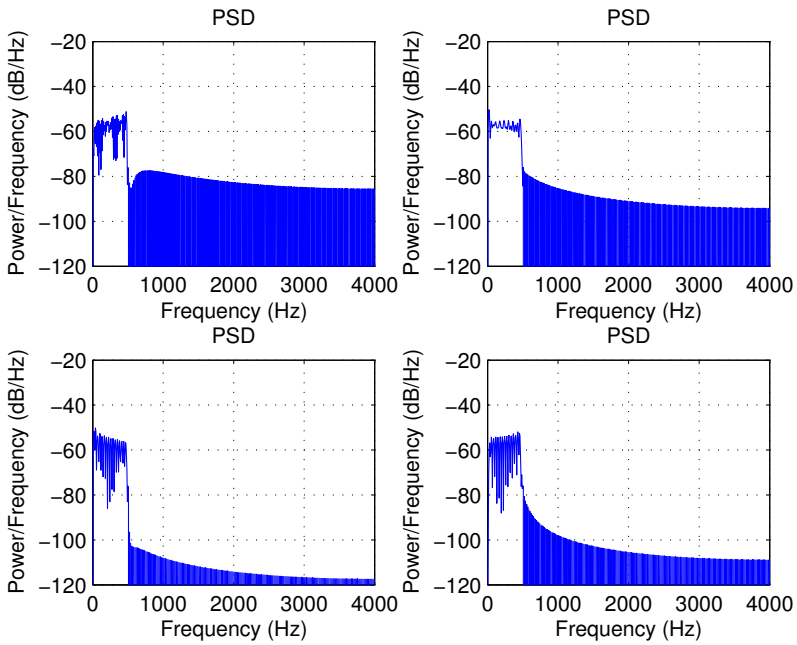

Figure 5.34: The PSD of four transmitted signals constructed from cosine functions, f_0=484Hz

Figure 5.35 shows the power spectrum densities of four transmitted signals with WLJ functions when $f_0 = 234Hz$

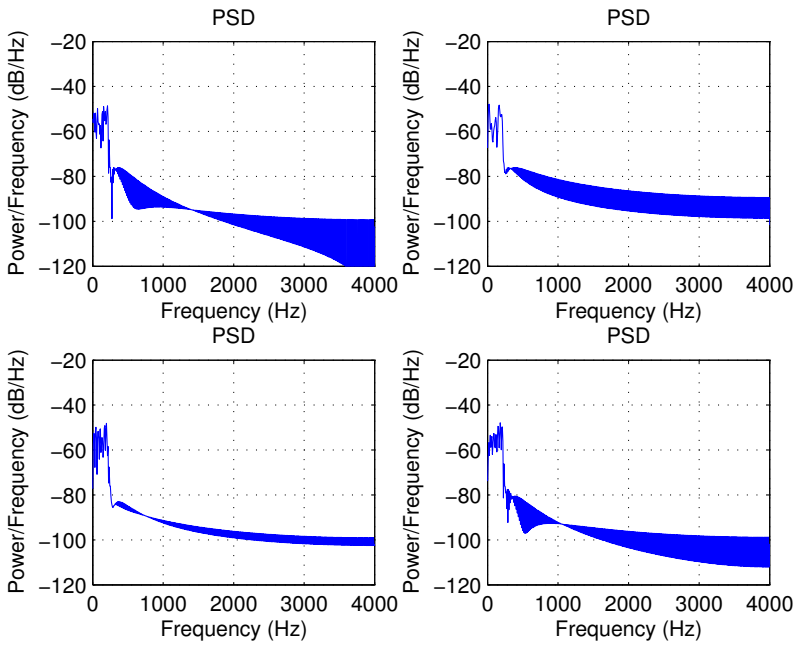

Figure 5.35: The PSD of four transmitted signals constructed from WLJ, f_0=234Hz

In this experiment, we observe that the designed waveforms by applying WLJ functions have the smallest essential bandwidth among three orthonormal bases.

5.3.2 Seeking minimum bandwidth using different orthonormal sets

In previous section as we put essential bandwidth in the constraint in arguement, the essential bandwidth is not minimum.

Now, we examine the case when given (i) the prescribed error between the signal covariance and the identity matrices, (ii) the sidelobe constraints in the ambiguity, and (iii) the sidelobe in the stop-band, we seek for the minimum bandwidth of the

transmission signal synthesized using the three orthonormal bases. We want to compare the minimum bandwidths in the use of the Walsh, cosine, and WLJ functions as signal synthesizing sets for given constraints that $\varepsilon = 10^{-2}$, $\Delta_f = 10^{-2}$, $\epsilon(1,0) = \alpha M$ and $\epsilon(\tau,0) = (\alpha/2)M$. We vary α from 0.1 to 0.4, and $\varepsilon = 10^{-2}$. In this experiment we measure the error between covariance and identity in RD. Figure 5.36. illustrates the comparison of the respective minimum bandwidths for various values of $\epsilon_{\tau,0}$.

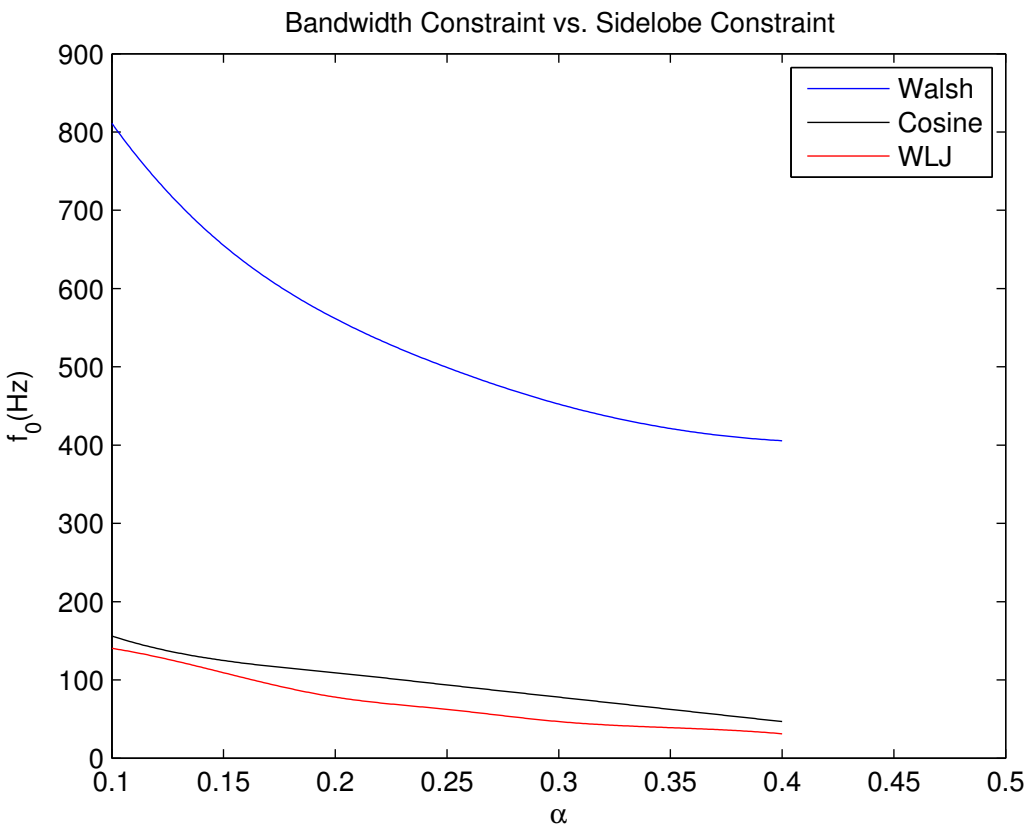

Figure 5.36: Bandwidth constriants vs. sidelobe constriants using Walsh, cosine and WLJ sets, $\varepsilon = 10^{-2}$

If we change ε to 10^{-5} then we obtain Figure 5.37. This illustrates the comparison

of the respective minimum bandwidths for various values of $\epsilon(\tau, 0)$.

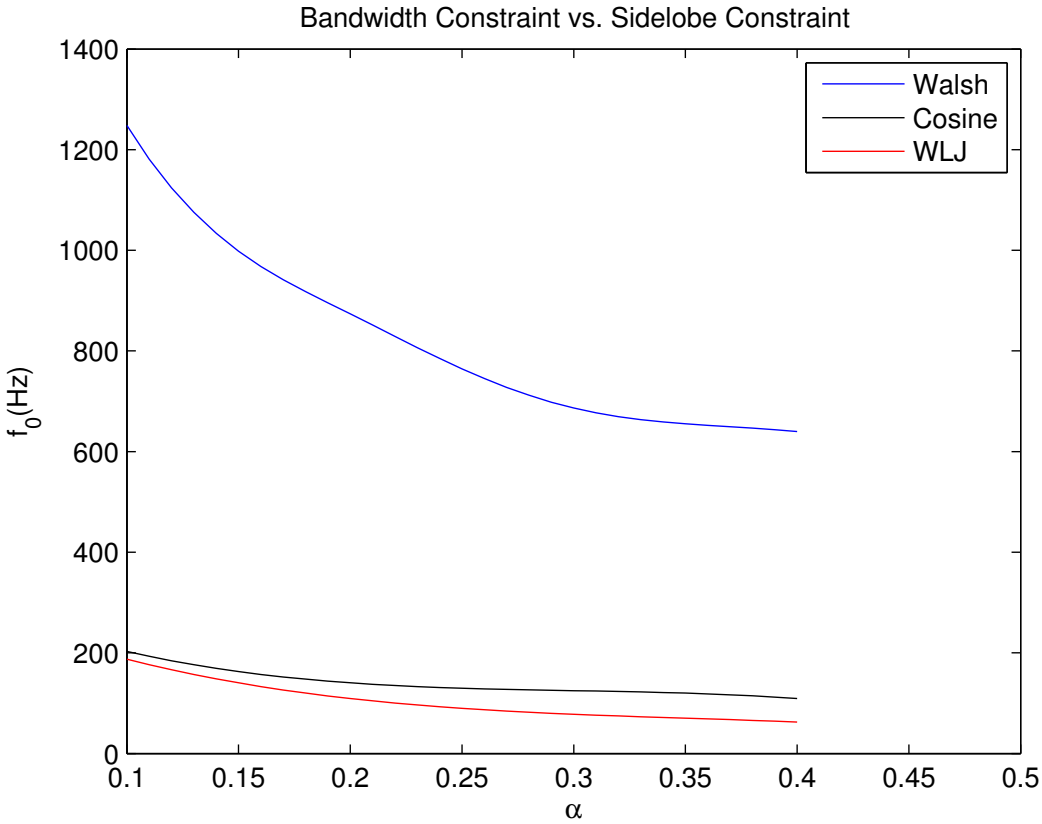

Figure 5.37: Bandwidth constriants vs. sidelobe constriants using Walsh, cosine and WLJ sets, $\varepsilon = 10^{-5}$

It can be observed that the signal synthesized using WLJ functions achieves the lowest bandwidth while satisfying all the constraints. Using sinusoids comes at a close second. It is observed that the use of Walsh functions requires a bandwidth far greater than either the use if the WLJ set or the cosine set. This can be easily understood since Walsh functions are rectangular functions having a sinc shaped roll-off in the frequency domain.

Chapter 6

Conclusion and Future Work

We considered the design of transmission signal for MIMO radar systems focusing on minimizing the distance between signal covariance matrix and a desired covaraince matrix while suppressing sidelobes of ambiguity functions with any non-zero time delay or Doppler frequency shift. We argue that since covariance matrices are not freely structured but are positive semi-definite and Hermitian-symmetric, the true distance should be formulated in terms of a Riemannian distance (RD) on the manifold of positive semi-definite and symmetric matrices. The design based on the RD measure was shown to yield a signal having higher estimation accuracies in both target location and target velocity. The optimum design using RD measure also offers much faster convergence. Furthermore, if the WLJ orthonormal set is used as the waveform-synthesizing basis, the transmission signal not only will satisfy the ambiguity requirements but it will also prossess very low bandwidth.

In numerical experiments, we have shown that the design based on the RD measure has faster convergence and better estimation performance compare to the design based on thenED measure. We have presented an explaination on fast convergence of the RD

measure. The design based on the RD measure also has better estimation performance as it has smaller cross correlation between any two antennas and also smaller elements of the sidelobe ambiguity matrices. In the future work, to understand fully the value of using RD metric, we need to carry out experiments to reveal the reason behind the improved estimation performance of the design based on RD. Next, we can make the sidelobe constraint more stringent in the optimization. In (2.28), we emphasize on the good auto-correlation properties so that we minimize the distance between estimated covariance of transmitted signals and the desired covariance in the objective and constriant on the sidelobes. In the future work, we can try to minimize the sidelobes of ambiguity functions and constraint on the distance between covariance estimation and desired covariance in order to emphasize the good cross-correlation properties. Furthermore, we can compare the ambiguity functions with and without sidelobe constraints to find the effect of sidelobe constraint on the design.

Bibliography

[1] Qu Jin, Zhi-Quan Luo, and Kon Max Wong. An optimum complete orthonormal basis for signal analysis and design. *IEEE Transactions on Information Theory*, 40(3):732–742, 1994.

[2] Harry L Van Trees. *Detection, estimation, and modulation theory*. John Wiley & Sons, 2004.

[3] Louis Nicot Ridenour. *Radar system engineering*, volume 1. Dover Publications, 1965.

[4] Jian Li, Luzhou Xu, Petre Stoica, Keith W Forsythe, and Daniel W Bliss. Range compression and waveform optimization for MIMO radar: A Cramer–Rao bound based study. *IEEE Transactions on Signal Processing*, 56(1):218–232, 2008.

[5] Chun-Yang Chen. *Signal processing algorithms for MIMO radar*. PhD thesis, California Institute of Technology, 2009.

[6] Hao He, Petre Stoica, and Jian Li. Designing unimodular sequence sets with good correlations–including an application to MIMO radar. *IEEE Transactions on Signal Processing*, 57(11):4391–4405, 2009.

[7] Alexander M Haimovich, Rick S Blum, and Leonard J Cimini. MIMO radar with widely separated antennas. *IEEE Signal Processing Magazine*, 25(1):116–129, 2008.

[8] Jian Li and Petre Stoica. MIMO radar with colocated antennas. *IEEE Signal Processing Magazine*, 24(5):106–114, 2007.

[9] Yang Yang and Rick S Blum. Minimax robust MIMO radar waveform design. *IEEE Journal of Selected Topics in Signal Pocessing*, 1(1):147–155, 2007.

[10] Benjamin Friedlander. Waveform design for MIMO radars. *IEEE Transactions on Aerospace and Electronic Systems*, 43(3):1227–1238, 2007.

[11] J Oppermann and Branka S Vucetic. Complex spreading sequences with a wide range of correlation properties. *IEEE Transactions on Communications*, 45(3):365–375, 1997.

[12] Petre Stoica, Jian Li, and Yao Xie. On probing signal design for MIMO radar. *IEEE Transactions on Signal Processing*, 55(8):4151–4161, 2007.

[13] Yong-Chao Wang, Xu Wang, Hongwei Liu, and Zhi-Quan Luo. On the design of constant modulus probing signals for MIMO radar. *IEEE Transactions on Signal Processing*, 60(8):4432–4438, 2012.

[14] Jian Li, Petre Stoica, and Xiayu Zheng. Signal synthesis and receiver design for MIMO radar imaging. *IEEE Transactions on Signal Processing*, 56(8):3959–3968, 2008.

[15] Kon Max Wong, Z-Q Luo, and Qu Jin. Design of optimum signals for the

simultaneous estimation of time delay and doppler shift. *IEEE Transactions on Signal Processing*, 41(6):2141–2154, 1993.

[16] Chun-Yang Chen and PP Vaidyanathan. MIMO radar ambiguity properties and optimization using frequency-hopping waveforms. *IEEE Transactions on Signal Processing*, 56(12):5926–5936, 2008.

[17] Yili Li and Kon Max Wong. Riemannian distances for signal classification by power spectral density. *IEEE Journal of Selected Topics in Signal Processing*, 7(4):655–669, 2013.

[18] Mingyi Hong, Meisam Razaviyayn, Zhi-Quan Luo, and Jong-Shi Pang. A unified algorithmic framework for block-structured optimization involving big data: With applications in machine learning and signal processing. *IEEE Signal Processing Magazine*, 33(1):57–77, 2016.

[19] Amari Shun-ichi. *Differential-geometrical methods in statistics*, volume 28. Springer Science & Business Media, 2012.

[20] Sylvestre Gallot, Dominique Hulin, and Jacques Lafontaine. *Riemannian geometry*, volume 3. Springer, 1990.

[21] Jia Xu. A riemannian distance in signal design for mimo radar. Master's thesis, McMaster University, 2014.

[22] M Grant, S Boyd, and Y Ye. CVX. Matlab software for disciplined convex programming, ver. 2.0, build 870, 2012.

[23] Joseph L Walsh. A closed set of normal orthogonal functions. *American Journal of Mathematics*, 45(1):5–24, 1923.

[24] Aurelien Tcheghoyz, Sebastian Sattler, and Helmut Graby. Mixed-signal testing using walsh functions. In *Mixed-Signals, Sensors, and Systems Test Workshop, 2009. IMS3TW'09. IEEE 15th International*, pages 1–8. IEEE, 2009.

[25] Lewis Embree Franks. *Signal theory.* Dowden & Culver, 1981.

[26] Athanasios Papoulis. Fourier integral and its applications. 1960.